Original Article

Contextual relationship between mechanical heterogeneity and dyking: constraints from magma emplacement dynamics of the ca. 2.21 Ga Anantapur–Kunigal mafic dyke swarm, Dharwar Craton, India

Srinjoy Datta, Amiya K. Samal [ID], Sayandeep Banerjee [ID] and Rajesh K. Srivastava [ID]

Department of Geology, Banaras Hindu University, Varanasi, India

Abstract

Mafic dykes are typically emplaced through primary hydraulic fracturing of undeformed crust or may make use of pre-existing crustal inhomogeneities, representing the plumbing systems of a large igneous province. The Eastern Dharwar Craton has dense exposures of several generations of Paleoproterozoic mafic dyke swarms ranging from ca. 2.37 Ga to ca. 1.79 Ga. Herein, using anisotropy of magnetic susceptibility fabric data of mafic dykes and associated host granites, the emplacement systematics of the NW- to W-trending ca. 2.21 Ga Anantapur–Kunigal dyke swarm, displaying a radiating geometry, have been studied to understand magma flow dynamics. A low-angle relationship between the silicate and opaque fabrics and good correlation with magnetic lineation, identified via petrographic studies and shape preferred orientation analyses of multiple oriented thin sections, suggest a primary flow-related magnetic anisotropy for the studied dyke samples. The classic subparallel relationship between the trend of the dyke planes and magnetic fabric of the associated host granites suggests that the radiating geometry of the ca. 2.21 Ga dyke swarm was supported by a favourable pre-existing structural grain of the country rock. We interpret the magma for the studied dyke swarm was fed laterally from a distant plume. It was emplaced as laterally propagating primary dyke fractures as well as injected into the pre-existing subparallel crustal inhomogeneities. Corroborating all these inferences, a detailed emplacement model for ca. 2.21 Ga Anantapur–Kunigal dyke swarm is also proposed.

1. Introduction

Large igneous provinces (LIPs) are widespread intraplate mafic–ultramafic magmatic events, having volumetric extent greater than 0.1 Mkm^3, emplaced as a short duration pulse or multiple pulses over a maximum of a few tens of Myr (cf. Ernst, 2014; Ernst & Youbi, 2017; Srivastava *et al.* 2022a). Mafic dyke swarms and sill complexes act as the plumbing system for LIPs, channelling magma from great depths to the surface of the Earth. Mafic dyke swarms typically serve as the surficial manifestations of highly eroded Precambrian LIPs, and they provide an opportunity to examine magma flow dynamics and emplacement systematics in a LIP. The dynamics of magma movement within the dyke can be effectively and precisely studied using anisotropy of magnetic susceptibility (AMS), an efficient method for identifying the preferred orientation of magnetic minerals in rocks, representing its magnetic fabric (Tarling & Hrouda, 1993). In undeformed and unmetamorphosed igneous rocks, the major magnetic fabric frequently mimics the direction of magma flow. Therefore, AMS is especially useful to retrieve valuable information about the magma flow dynamics of igneous rocks (Ernst, 1994; Hastie *et al.* 2014), which often display weak and inconspicuous magmatic fabrics.

The emplacement of a mafic dyke can be observed as an active or passive intrusion. The former involves primary hydraulic fracturing in the undeformed country rock, whereas the latter takes advantage of the pre-existing inhomogeneities in the crust (Jourdan *et al.* 2006), i.e. change in lithology, fractures, foliations, faults and intra-terrane shear zones (Banerjee *et al.* 2022). Giant radiating dyke swarms are generally related to mantle plume-related tectonics (e.g., Ernst *et al.* 2001; Hou, 2012; Ernst, 2014). The emplacement of dykes is generally guided by ambient stress regimes; regional stress regimes are known to govern over greater distances from the plume centre, while local magmatic stress regimes have a stronger effect closer to the plume centre (Ernst *et al.* 2001; Hou, 2012). However, in both cases, the nature in which the host rock would respond to the imposed stress field would depend on the interrelationship of the ambient stress regime of the country rock and the new magmatic stress regime. Thus, to comprehend the emplacement mechanisms of dyke swarms, it is necessary to investigate and incorporate

the effect of the pre-existing stress regime. Pre-existing crustal inhomogeneities are products of an older stress regime in the country rock. Crustal inhomogeneities can have a variety of orientations ranging from horizontal to vertical. A horizontal to low angle inhomogeneity can change the local stress field, thereby modifying a propagating dyke path (Elshaafi & Gudmundsson, 2016), which in a majority of the cases act as a hindrance to dyke propagation, thereby several dykes become blind or non-feeder by nature (Gudmundsson, 2006). On the contrary, high-angle anisotropies, represented by normal faults, extension fractures or high-angle shears (thrust or strike-slip), influence the local stress regime constructively, thereby facilitating dyke propagation along the fault plane, irrespective of the stiffness of the fault (Elshaafi & Gudmundsson, 2016). Due to the tensile stress environment that surrounds normal faults (Cadman *et al.* 1993; Torres-Hernández *et al.* 2006) and extension fractures, dykes favour these possible propagation channels over thrust faults (Misra & Mukherjee, 2017), which have a compressive stress environment around them. The strike-slip setting, on the other hand, has displayed dyke intrusion into the primary shear fracture and accompanying hybrid fractures such as riedel fractures and Y and P fractures (e.g., Xu *et al.* 2013; Maity & Banerjee, 2022). Therefore, understanding the existing mechanical heterogeneity in the crust is crucial to infer the dyke emplacement mechanism.

The Dharwar Craton, an integral part of the DHABASI megacraton (Srivastava *et al.* 2022b), provides a classic example of Archean–Proterozoic processes preserved in its rocks and its association with Superia, Sclavia, Columbia and Rodinia super-continents is established (Bleeker & Ernst, 2006; French & Heaman, 2010). Hence, understanding its geodynamic evolution is crucial for comprehending global Precambrian tectonics. The Dharwar Craton lithosphere is intruded by several generations of Proterozoic mafic dyke swarms spanning from ca. 2.37 Ga to ca. 1.79 Ga (cf. Samal *et al.* 2021a; Srivastava *et al.* 2022b). Most of these dyke swarms are well constrained in terms of their paleomagnetism (Piispa *et al.* 2011; Kumar *et al.* 2012, 2015; Pivarunas *et al.* 2018; Pivarunas & Meert, 2020 and reference therein), geochronology (Halls *et al.* 2007; French & Heaman, 2010; Srivastava, 2011; Kumar *et al.* 2012, 2015; Nagaraju *et al.* 2018; Söderlund *et al.* 2019; Sarma *et al.* 2020; Parashuramulu *et al.* 2021) and geochemistry (Kumar *et al.* 2012; Srivastava *et al.* 2014a, 2014b; 2015; Nilsson *et al.* 2013; Srivastava *et al.* 2020; Samal *et al.* 2019a, 2019b). However, research on the emplacement systematics and magma flow dynamics of these swarms are limited and restricted (e.g., Kumar *et al.* 2015; Nagaraju & Parashuramulu, 2019; Ramesh *et al.* 2020; Datta *et al.* 2023). Moreover, earlier geochemical studies (Srivastava *et al.* 2014a, 2014b; 2015; Samal *et al.* 2021b, 2021c; Parashuramulu *et al.* 2022) have unanimously characterized these dykes as unmetamorphosed and undeformed. This makes the dykes of the Dharwar Craton even better candidates for studying the primary magma flow dynamics. The ca. 2.21 Ga Anantapur–Kunigal dyke swarm has a more comprehensive spatial extent covering the entire Eastern Dharwar Craton (EDC), and it displays a spectacular radiating geometry with two sub-swarms spread over the northern and central sectors of the EDC (cf. Söderlund *et al.* 2019). Therefore, this ca. 2.21 Ga mafic dyke swarm has been targeted in the present study. To gain a comprehensive understanding of dyking mechanism and its relation to regional stress fields, the dykes of this swarm are compared with the host rock, fracture patterns and existing intra-terrane shear zones in the EDC. We have also conducted shape preferred orientation (SPO) analyses of the silicate and opaque

fabrics in several oriented thin sections of the dyke samples and compared them with the respective magnetic fabrics to validate the primary nature of the observed magnetic anisotropy. Therefore, the objectives of the present work are broadly three-fold: (i) to present preliminary magnetic fabric data for the ca. 2.21 Ga Anantapur–Kunigal dyke swarm and associated host granites, (ii) to observe the variation in magnetic anisotropy data (if any) between the two sub-swarms and (iii) to study the magma flow direction within the dyke fractures, thereby to understand the interrelationship of the pre-existing shear systems and regional stress fields, with the stress regime related to the dyke emplacement. By integrating all the generated datasets, we propose a possible emplacement model for the ca. 2.21 Ga Anantapur–Kunigal dyke swarm, which can be replicated to analogous mafic dyke swarms in the other cratons of the Indian shield in general and Dharwar Craton in particular.

2. Regional geology

The Dharwar Craton is a low-grade granite–greenstone terrain. Many earlier studies (e.g., Naqvi & Rogers, 1987; Li *et al.* 2018; Jayananda *et al.* 2018, 2020; and references therein) have explored its intricate geology. Broadly, the craton has an Archean tonalite–trondhjemite–granodiorite gneissic basement (ca. 3.5–3.3 Ga; Peucat *et al.* 1993), which are overlain by two generations of supracrustal greenstone belts – the older Sargur group (ca. 3.58–3.0 Ga; Peucat *et al.* 1995; Jayananda *et al.* 2008) and the younger Dharwar supergroup (ca. 2.9–2.6 Ga; Taylor *et al.* 1984; Kumar *et al.* 1996). Further, the craton is home to ca. 2.6–2.5 Ga Potash-rich granites, which are well documented as the last magmatic episode before its stabilization (Jayananda *et al.* 2020). Based on the difference in thermal and accretionary history, the craton is classically divided into two sub-blocks, i.e., the Eastern and Western Dharwar Craton (EDC and WDC), along the Chitradurga Shear Zone (Chadwick *et al.* 2000), which is a prominent shear zone running continuously along the NNW-trending Chitradurga Greenstone belt (Fig. 1a). The EDC is further divided into Central and Eastern Dharwar Craton, along the Kolar–Kadiri–Penakacherla–Kushtagi–Hungund greenstone belt (Jayananda *et al.* 2013; Dey, 2013).

The lithosphere of the Dharwar craton has experienced several episodes of voluminous magmatism in the Paleoproterozoic era. These are represented by distinct craton-scale mafic dyke swarms spanning from ca. 2.37 Ga to ca. 1.79 Ga, which include (i) ca. 2.37–2.36 Ga NE- to ESE-trending Bangalore–Karimnagar dyke swarm, (ii) ca. 2.26–2.25 Ga N- to NNE-trending Ippaguda–Dhiburahalli dyke swarm, (iii) ca. 2.22 Ga N- to NNW-trending Kandlamadugu dyke swarm, (iv) ca. 2.21 Ga NW- to WNW-trending Anantapur–Kunigal dyke swarm, (v) ca. 2.18 Ga NW- to WNW-trending Mahbubnagar–Dandeli dyke swarm, (vi) ca. 2.08 Ga N-, NW- and NE-trending Devarabanda dyke swarm, (vii) ca. 1.89–1.88 Ga E- to ENE-trending Hampi dyke swarm along with associated Pulivendula sills and (viii) ca. 1.79 Ga NW-trending Pebbair dyke swarm (cf. French & Heaman, 2010; Söderlund *et al.* 2019; Samal *et al.* 2019b; 2021a; and references therein). These dyke swarms have been studied in detail throughout the past two decades and are considered as part of different LIP events (Samal *et al.* 2019b). Various geochemical and paleomagnetic studies (Halls *et al.* 2007; French & Heaman, 2010; Srivastava, 2011; Kumar *et al.* 2012; Pivarunas *et al.* 2018; Söderlund *et al.* 2019) on these dyke swarms have established their plume related origin and have even demarcated their potential plume centres (Ernst & Srivastava,
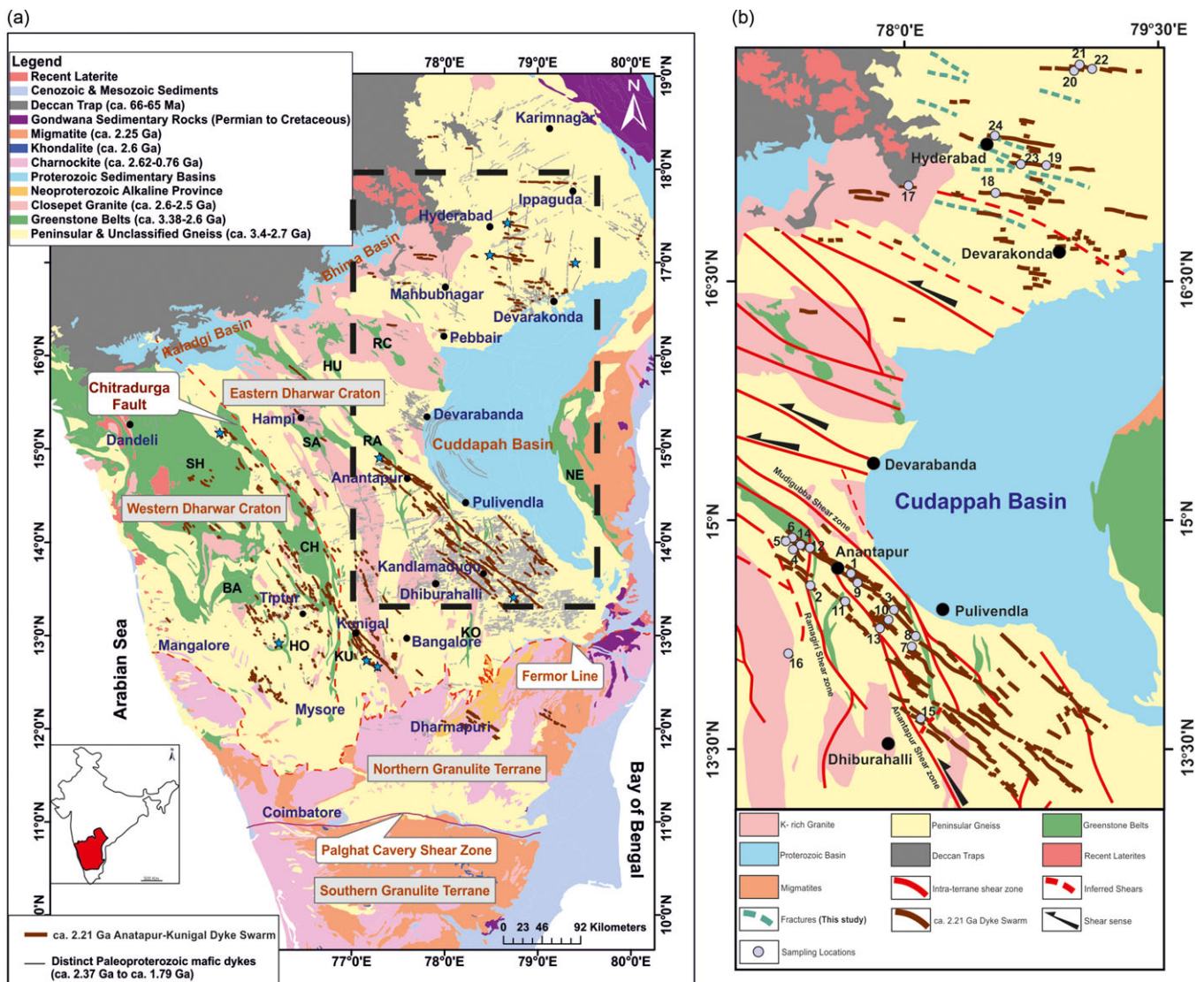
Figure 1. (Colour online) (a) Regional map of Dharwar Craton with Paleoproterozoic dyke swarms after French and Heaman (2010) and Samal *et al.* (2019a). The study area is denoted by a rectangle. (b) Detailed map of the study area, displaying the ca. 2.21 Ga Anantapur–Kunigal dyke swarm (Samal *et al.* 2019a), the intra-terrane shear zones (Chardon *et al.* 2008) and sampling locations. The numbers used at the sampling location are the same as the serial numbers in Tables 1a and 1b. Host granite samples were also collected from sampling locations 3, 10, 11, 12 and 24. Greenstone belts: BA – Bababudan; CH – Chitradurga; HO – Holenarsipur; HU – Hutti; KO – Kolar; KU – Kunigal; NE – Nellore; RA – Ramagiri; RC – Raichu; SA – Sandur; SH – Shimoga. The blue stars (dated samples) are taken from French and Heaman (2010); Nagaraju *et al.* (2018); Söderlund *et al.* (2019), Yadav and Sarma (2021). The spatial extent of Dharwar Craton is marked in red in the map inset. Although the northern extent of the craton is not well constrained due to the cover of Deccan volcanics in the north.

2008; French & Heaman, 2010; Kumar *et al.* 2012, 2015; Nagaraju *et al.* 2019; Ramesh *et al.* 2020; Samal *et al.* 2021b, 2021c; Yadav *et al.* 2020, 2021 and Parashuramulu *et al.* 2022 among several others). Their exposures are denser in the EDC relative to WDC, likely due to differences in their crustal lithologies or a weaker lithosphere beneath the EDC or proximity of the plume centre to the EDC (cf. Chardon *et al.* 2002; 2008; Chardon & Jayananda, 2008; Söderlund *et al.* 2019).

3. Methodology

3.a. Sampling and field observations

The NW- to WNW-trending ca. 2.21 Ga Anantapur–Kunigal dyke swarm displays a radiating geometry (one sub-swarm is NW-trending and another is WNW-trending) as confirmed by its

available geochronological (French & Heaman, 2010) and geochemical data (French & Heaman, 2010; Srivastava *et al.* 2015; Samal *et al.* 2021b) (see Fig. 1a, b). Samples have been collected from 24 locations from this swarm, covering both the sub-swarms from central and northern parts of the EDC, in and around Anantapur and Hyderabad districts, respectively (Fig. 1b). The sampled dykes in the central part of the EDC are largely from the NW-trending sub-swarm and those in the northern part are from the WNW-trending sub-swarm. We have used the notations sub-swarm-1 for NW-trending dykes and sub-swarm-2 for WNW-trending dykes throughout this work. Sampling from both the sub-swarms (trends) allowed us to study the spatial variation (if any) of the magnetic susceptibility data throughout the entire dyke swarm. Some dykes show distinct chilled margins in a vertical profile (Fig. 2a). Oriented block samples were collected from the chilled margins (wherever visible) or otherwise close to the dyke
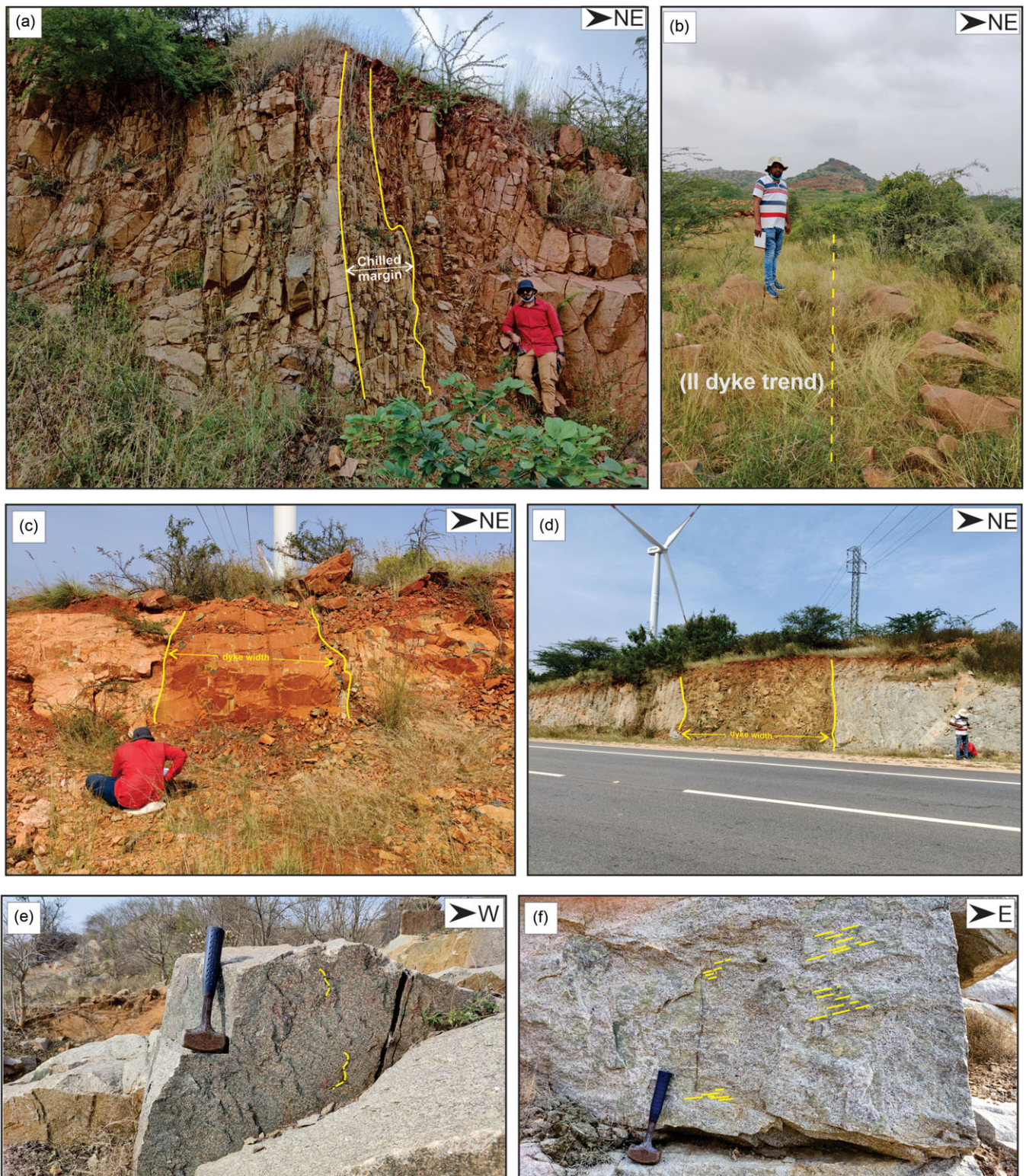
Figure 2. (Colour online) Field photographs of the ca. 2.21 Ga mafic dyke swarm. (a) Road-cut vertical section of dyke exposing highly jointed cubic blocks. The trend of the dyke is 302°. It displays a distinct chilled margin (marked in yellow). Oriented samples were collected from such chilled margins, wherever they were visible, as they best preserved the magnetic fabric. (b) Outcrop of boulders of a dyke exposed north of Anantapur district Andhra Pradesh. The trend of the dyke is marked in yellow and is along 310°. (c, d) Vertical section of NW-trending dyke showing distinct contact with country rock. The sub-vertical dyke margins are marked in yellow. (e) Slicken sides on host granite along 270°, depicting the E–W-trending shear zone located near Nawabpet, Telangana. (f) Slicken sides on host granite represented by preferred orientation minerals along 270°, the location was in the vicinity of 2(c).

margins, as they host the best-preserved magnetic flow fabrics. Each of our collected dyke samples represents a single margin of a mafic dyke exposure. However, due to the lack of continuous outcrops and barely visible dyke borders in several of our sampling locations, sampling over the width of the dykes was not feasible. Based on megascopic and petrographic investigations, sampled dykes were classified as medium- to coarse-grained dolerites. Further, oriented block samples were also collected from the associated host granites, close to locations of studied mafic dykes, from five locations within the study area. Their magnetic fabrics were determined to identify the structural grain of the country rock, which was intruded by the dyke swarm. We have also determined the orientation data of several fracture systems (see Supplementary Table S1) and mesoscopic shears in the host granites to understand the effect of the pre-existing regional stress fields of the country rock on the emplacement systems of the studied dyke swarm.

3.b. AMS study

A total of 16 and 8 mafic dykes were sampled from the sub-swarm-1 and 2, respectively. Further, 187 specimens in the form of cylindrical cores (2.5 cm diameter and 2.2 cm height) and cubes ($2 \times 2 \times 2$ cm dimensions) were extracted from the oriented block samples of these mafic dykes. In addition, 26 cylindrical cores were retrieved from 5 host granite samples using a static corer and slab saw cutter. These specimens were subjected to low-field magnetic anisotropy studies using a MFK2-FA multifunction Kappabridge instrument (AGICO Co. Ltd., Czech, Republic) installed at the Laboratory for Analysis of Magnetic and Petrofabric (LAMP) in the Department of Geology, Banaras Hindu University, Varanasi. The instrument has a sensitivity of 2×10^{-8} SI. The analyses were conducted in a magnetic field of 200 A/m and a frequency of 976 Hz. Further processing of the data was performed using the Anisoft 5.1.08 software.

The variation in magnetic susceptibility can be mathematically expressed as a second-rank tensor and can be geometrically visualized as a triaxial ellipsoid (Tarling & Hrouda, 1993; Dunlop & Özdemir, 1997), which is referred to as the susceptibility ellipsoid. Its three principal axes are denoted by K_1, K_2 and K_3, which represent the maximum, intermediate and minimum axes, respectively (Hrouda, 1982; Borradaile, 1991). The magnitudes of the susceptibility axes were obtained from the abovementioned analyses (Tables 1a and 1b). These were used to calculate the mean bulk susceptibilities (K_m) via equation (1):

$$K_m = \frac{(K_1 + K_2 + K_3)}{3} \quad (1)$$

Further, they were used to calculate other parameters like the degree of magnetic foliation – F (equation 2), magnetic lineation – L (equation 3), shape parameter – T (equation 4) and degree of Anisotropy – P_j (equation 5). The abovementioned equations are discussed as follows (Khan, 1962; Jelinek, 1981):

$$F = \frac{K_2 - K_3}{K_m} \quad (2)$$

$$L = \frac{(K_1 - K_2)}{K_m} \quad (3)$$

$$T = \frac{2(\eta_2 - \eta_3)}{(\eta_1 - \eta_3)} - 1 \quad (4)$$

where $\eta_1 = \ln K_1$, $\eta_2 = \ln K_2$ and $\eta_3 = \ln K_3$ (Jelinek, 1981).

$$P_j = \exp \sqrt{2\{(\eta_1 - \eta_m)^2 + (\eta_2 - \eta_m)^2 + (\eta_3 - \eta_m)^2\}} \quad (5)$$

where $\eta_m = \frac{\eta_1 + \eta_2 + \eta_3}{3}$.

The degree of Anisotropy (P_j) represents the magnitude of the magnetic fabric or the susceptibility ellipsoid. It is often considered as the measure of the intensity of strain suffered by the studied rock. On the other hand, the shape parameter (T) determines the prolate ($-1 < T < 0$) or oblate ($0 < T < 1$) shape of the susceptibility ellipsoid, which suggest the nature of the stress regime (constrictional or flattening).

3.c. Mineral chemistry

All the collected samples were studied petrographically. Further, two samples from the two sub-swarms, with highest K_m values, were selected for scanning electron microscopy and energy dispersive X-ray spectroscopy (SEM-EDS) and electron probe microanalyses (EPMA) to identify the phases responsible for the induced magnetization. These analyses were done at the DST-SERB National facility, Department of Geology, Banaras Hindu University, Varanasi. Sections from the selected samples were cut along the K_1-K_2 plane, i.e., the magnetic foliation plane, to characterize the relation between the SPO of the opaque and plagioclase grains and the magnetic lineation (K_1). The polished thin sections were coated with a 20 nm thin carbon layer using the LEICA EM ACE-200 instrument for preliminary SEM-EDS analyses, followed by detailed EPMA analyses of the opaque phases.

SEM-EDS analyses and back scattered emission (BSE) imaging were done using a Carl Zeiss EVO18 Research Model. BSE imaging of the carbon-coated thin sections was done with a working distance of 8 mm and a voltage of 20 KV. Subsequent EDS analysis was done for the opaque phases as a semi-quantitative method to estimate the chemistry of the opaque phases in the polished thin sections.

EPMA analyses further confirmed the preliminary measurements by SEM-EDS. Herein, the major elemental composition of the opaque phases (see Supplementary Table S2) in the selected thin sections was conducted in the CAMECA SX-five electron microprobe using wave-length dispersive spectrometry. LaB6 crystal was used as a source to generate an electron beam. The diameter of the beam was approximately 1 μm. The instrument was run at a beam current of 10 nA and an acceleration voltage of 15 KV. The counting times were set for 30 seconds at the peak and 15 seconds on either side in the background. Natural diopside, peridot, almandine and magnetite were used as standards for efficient detection of the elemental composition of the opaque phases. SxSAB version 6.1 and SX-Results software of CAMECA were used for routine calibration, acquisition, quantification and further data processing. The entire dataset was treated with X-PHI matrix correction. The instrument provided an analytical precision of better than 1% for major element oxides. BSE images for the opaque phases were also captured to identify chemical variation and exsolution signatures in the opaque phases. The mineral chemical data were further processed for the characterization and classification of the opaque phases.

Table 1a. AMS directions of ca. 2.21 Ga Anantapur–Kunigal dyke swarm

Sl. no.	Sample no.	Location		Trend	K_m	L	F	P_j	T	K_1		K_2		K_3		K_1-K_2 plane	ζ	Fabric type
		Lat (°)	Long (°)		μSI Units					D (°)	I (°)	D (°)	I (°)	D (°)	I (°)	(Dip amt.-Dip dir.)		
Sub-swarm-1																		
1	EDC20/12A (6)	14°46'6.4"N	77°32'10.5"E	310	9366	1.011	1.01	1.021	0.02	0.3	47.7	114.5	20.4	219.7	35.1	54.8–039.6	0.4	Subparallel
2	EDC20/22C (8)	14°39'33.43"N	77°27'3.02"E	295	4762	1.005	1.006	1.011	0.13	287.3	43.9	76.4	41.7	181.3	16	73.9–001.2	23.8	Subparallel
3	EDC20/32A (7)	14°29'47.00"N	77°52'39.00"E	321	16220	1.027	1.01	1.037	−0.42	93.7	25.5	344.3	34.8	211.5	44.4	45.6–031.4	19.6	Subparallel
4	EDC21/2A (7)	14°52'37.2"N	77°18'56.1"E	310	2332	1.007	1.006	1.013	−0.172	301.3	6.7	42.4	58.5	207.3	30.6	47.5–025.1	14.9	Subparallel
5	EDC21/3 (9)	14°53'18.39"N	77°17'57.85"E	310	2023	1.009	1.013	1.023	0.164	105.3	2.6	11.5	54.7	197.1	35.2	54.8–017.1	22.9	Subparallel
6	EDC21/4 (8)	14°53'33.20"N	77°18'55.29"E	300	39810	1.018	1.006	1.025	−0.503	217.6	49	121	5.7	26.1	40.4	49.5–206.1	3.9	Subparallel
7	EDC21/11 (8)	14°15'24.68"N	78° 4'6.27"E	315	6547	1.004	1.005	1.009	0.45	146.5	31.1	306.9	57.4	51	8.8	81.0–231.0	6	Subparallel
8	EDC21/12 (9)	14°15'38.74"N	78° 4'34.51"E	325	7157	1.014	1.022	1.037	0.241	208.3	40.8	299.9	1.8	32	49.1	40.8–211.9	23.1	Subparallel
9	EDC20/10 (7)	14°44'26.9"N	77°33'19"E	310	6142	1.016	1.003	1.021	−0.643	275.7	1.3	17.4	83.5	185.6	6.3	83.5–005.5	34.5	Oblique
10	EDC20/33A (7)	14°26'37.60"N	77°50'37.70"E	323	16460	1.018	1.028	1.047	0.285	196.7	12	296.9	40.1	93.3	47.4	42.5–273.3	40.3	Oblique
11	EDC20/37A (8)	14°30'21.10"N	77°37'48.80"E	328	3281	1.013	1.02	1.034	0.206	84.8	43.3	181.7	7.3	279.2	45.8	44.2–099.2	41.2	Oblique
12	EDC21/6A (7)	14°53'33.85"N	77°22'22.24"E	305	3732	1.013	1.013	1.026	−0.021	127.9	21.4	225.5	18.5	352.8	61	28.9–172.7	42.3	Oblique
13	EDC20/35 (8)	14°23'38.40"N	77°49'2.30"E	290	4236	1.007	1.013	1.021	−0.083	358.5	55.3	252.4	10.9	155.4	32.5	57.5–335.3	44.7	Oblique
14	EDC21/5 (8)	14°53'26.76"N	77°19'36.03"E	320	14130	1.026	1.015	1.041	−0.263	66.8	15.5	207.9	70.4	333.5	11.8	78.2–153.5	76.5	Perpendicular
15	EDC21/21 (9)	14° 2'44.31"N	78° 1'30.94"E	315	59260	1.027	1.02	1.048	−0.137	29.5	15.1	276.8	54.9	128.7	30.8	59.1–308.7	83.7	Perpendicular
16	EDC21/32 (8)	14°12'3.92"N	77°15'39.63"E	320	13220	1.011	1.005	1.017	−0.344	98.3	45.6	220.2	27.4	329	31.8	58.1–148.9	81.1	Perpendicular
Sub-swarm-2																		
17	EDC22/1A (7)	17° 5'38.22"N	78° 0'56.64"E	91	4409	1.013	1.011	1.025	−0.09	34.7	38.6	278.4	29	163	37.8	52.2–342.9	18.1	Subparallel
18	EDC22/10A (7)	17° 3'5.70"N	78°39'55.10"E	97	4024	1.005	1.006	1.012	0.135	119.1	23.3	231.8	41.8	8.5	39.2	50.8–188.5	1.5	Subparallel
19	EDC22/20A (9)	17°14'1.10"N	79° 2'36.80"E	95	10690	1.038	1.047	1.087	0.104	70.4	9.8	331.9	40.6	171.4	47.7	42.2–351.3	13.7	Subparallel
20	EDC22/30B (8)	17°51'11.20"N	79°12'24.00"E	105	22720	1.006	1.045	1.056	0.768	109.4	3.3	200.3	13.9	6.3	75.7	14.3–186.9	8.1	Subprallel
21	EDC22/31A (7)	17°51'26.50"N	79°12'42.50"E	105	1527	1.004	1.002	1.006	−0.243	42.4	50.1	311.7	0.5	221.3	39.9	50.1–041.2	26.2	Subparallel
22	EDC22/33 (8)	17°51'09.2"N	79°18'39.6"E	91	1965	1.007	1.004	1.011	−0.241	225.3	14.7	84.9	71.1	318.4	11.5	78.4–138.3	42.7	Oblique
23	EDC22/18 (8)	17°15'6.40"N	78°50'30.50"E	95	7243	1.045	1.034	1.081	−0.116	177.3	10.4	76.3	45.8	276.9	42.3	47.6–096.9	88.1	Perpendicular
24	EDC22/26A (9)	17°25'21.50"N	78°38'17.40"E	90	1892	1.003	1.002	1.005	−0.097	359.8	0.2	269.6	46.7	90	43.3	46.7–269.9	89.9	Perpendicular

K_1, K_2, K_3 are the maximum, intermediate and minimum magnetic susceptibility axes, respectively.
K_m is the bulk susceptibility.
L, F, P_j and T are magnetic lineation, magnetic foliation, corrected degree of anisotropy and Jellinek's shape parameter, respectively.
D and I are the declination and inclination in degrees.
K_1–K_2 plane is the magnetic foliation plane.
ζ is the angle between K_1 and K_2 plane and the dyke plane
The numbers in the parentheses are the number of specimen core/cubes analysed from each sample

Table 1b. AMS directions of associated host granites

| Sample no. | Location | | K_m | L | F | P_j | T | K_1 | | K_2 | | K_3 | | K_1-K_2 plane | Fabric Type |
	Lat (°)	Long (°)	μSI Units					D (°)	I (°)	D (°)	I (°)	D (°)	I (°)	(Dip amt.- Dip dir.)	
EDC20/32B (5)	14°29'47.00"N	7°52'39.00"E	498.7	1.044	1.141	1.201	0.505	269.5	70.3	178.3	0.4	088.2	19.7	70.3-268.1	(ii)
EDC20/33B (5)	14°26'37.60"N	77°50'37.70"E	7570	1.079	1.103	1.191	0.117	107.8	23	350.8	46.8	214.5	34.1	55.8-034.5	(i)
EDC20/37B (6)	14°30'21.10"N	77°37'48.80"E	2337	1.064	1.019	1.088	-0.543	237.2	3.9	130.7	76.6	328.1	12.8	77.1-148	(iii)
EDC21/6B (5)	14°53'33.85"N	77°22'22.24"E	535.9	1.01	1.027	1.038	0.445	058	21.6	323.5	11.2	207.9	65.4	24.5-027.8	(i)
EDC22/26B (5)	17°25'21.50"N	78°38'17.40"E	60	1.011	1.034	1.047	0.467	267.2	12.6	088	74.4	357.3	0.2	89.5-357.1	(i)

K_1, K_2, K_3 are the maximum, intermediate and minimum magnetic susceptibility axes, respectively.
K_m is the bulk susceptibility.
L, F, P_j and T are magnetic lineation, magnetic foliation, corrected degree of anisotropy and Jellinek's shape parameter, respectively.
D and I are the declination and inclination in degrees.
K_1–K_2 plane is the magnetic foliation plane.
The numbers in the parentheses are the number of specimen core/cubes analysed from each sample.

3.d. SPO Analyses

In order to ensure that the magnetic fabric can be used as prospective flow indicators, SPO analysis – a procedure to examine the relationship between the magnetic and magmatic fabrics – is necessary (Archanjo *et al.* 1995; Launeau & Cruden, 1998). It is also essential to compare the preferred orientation of the magnetic grains identified via petrography and digital image processing with the observed magnetic anisotropy directions, because AMS analyses measure the combined effect of all the ferro/ferri-magnetic and paramagnetic grains in a sample. This enables us to identify and avoid the effects of composite magnetic fabrics. Based on the characteristics of their magnetic fabrics (described later) and their high bulk susceptibilities, four mafic dyke samples were chosen (two from each sub-swarm). Three thin sections were cut from each sample along their respective magnetic foliation planes. Plagioclase laths exhibit a magmatic flow fabric in mafic dyke samples, whereas iron oxide phases contribute to a magnetic fabric (Wiegand *et al.* 2017; Das *et al.* 2021). The polished thin sections were studied under the microscope, and images were acquired for further digital processing in ImageJ 1.8.0 software (Rasband, 2012). The images were imported into the software, and after preliminary editing of the fractures and ambiguous grains, the geometry (long axes, short axes, aspect ratio and angle with the horizontal image axis) of the individual plagioclase and iron oxides grains were measured (see Supplementary Table S3). The grains displaying considerable shape anisotropy (aspect ratio ≥ 1.2) were included in the SPO analyses. Further, the azimuth of the plagioclase and the iron oxide grains were calculated from their angles with the horizontal image axis and plotted in rose diagrams. To better understand their interrelationship, the silicate and oxide roses were compared. They were then correlated with the magnetic anisotropy axes to evaluate the relationship between the observed magnetic lineation and the actual orientation of the magnetic grains in the magnetic foliation planes.

4. Results

4.a. Field observations

During multiple field-work campaigns, the studied mafic dykes were observed as outcrops mostly consisting of boulders whose margins were barely perceptible in plane profile (Fig. 2b), but in road-cut sections, they showed strongly jointed blocks. The dyke widths vary from ~6 m to several tens of metres. The majority of dykes displayed vertical to sub-vertical dips in road cut sections (Fig. 2a, c, and d); therefore, the dyke planes are considered to be vertical for the magnetic anisotropy studies in the subsequent sections. Further, evidence of shear structures like stretched mineral lineation and slicken surfaces in the host granites (Fig. 2e, f), especially in the northern part of the EDC, enabled the delineation of several E-trending intra-terrane shear zones in the northern part of the study area (Fig. 1b). The geometry of the fracture system developed in the host granitoids shows a range of dip from moderately inclined to vertical (23°–90°) (see Supplementary Table S1). However, the dominant dip lies between 80° and 90°. These fractures display varied trends, with dominant trends ranging from 110°–115° to 135°–140°, along with a considerable population between 050°and 075°.

4.b. Petrography

The mineralogy of the studied dyke samples includes typical euhedral to subhedral clinopyroxene and plagioclase grains
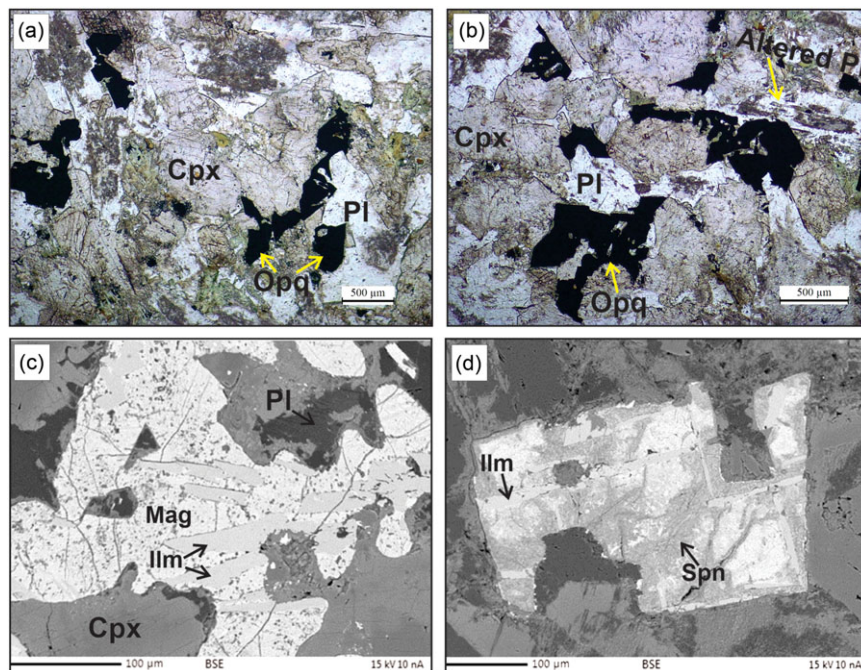
Figure 3. (Colour online) Photomicrographs and BSE images. (a) Photograph made in plane polarized light (PPL), demonstrating all the rock forming major and minor mineral phases in the rock, with distinct ophitic sub-ophitic texture. The secondary alteration phases are also observed in some of the plagioclase and clinopyroxene grains. (b) Photomicrograph displays the dominance of skeletal oxide grains along the K_1–K_2 plane. (c) BSE image displays distinct exsolution between ilmenite and magnetite phases. (d) The image displays ilmenite occurring as thin exsolution lamellae in a host of magnetite. The magnetite shows alteration to sphene.

displaying sub-ophitic relationships (Fig. 3a, b). Plagioclase laths show more significant variation in grain length, i.e., from 500 to 2000 μm compared to the clinopyroxenes (400–1000 μm). Some samples collected from the dyke margins display evidence of alteration. Plagioclase grains show a cloudy appearance, which is suspected to be altered to sericite (Fig. 3b). At the same time, the clinopyroxene grains show evidence of alteration to amphiboles at the grain boundaries (Fig. 3a, b). No signatures of deformation textures were observed in the detailed petrographic study, and the alterations observed were essentially local, probably due to chemical interaction with wall rocks and/or secondary fluids.

Characteristically, the main magnetic carrier mineral in dolerite dykes is titanomagnetite. In the studied dyke samples, titanomagnetite grains constitute up to 4% of the mode. The primary opaque phase, however, is comprised of ilmenite, which forms in the later stage of crystallization and occurs as euhedral to subhedral grains. In the studied dyke samples, ilmenite grain length ranges from a few micrometres to greater than 1000 μm. BSE imaging suggests marked exsolution between ilmenite and magnetite grains, which infers deuteric oxidation during the later cooling stages (Opdyke & Channell, 1996) (Fig. 3c, d). In some samples, the larger Fe-Ti oxides (>500 μm in length) display skeletal grains, which may be attributed to the faster cooling of the dykes. Some of the Fe-Ti Oxides have also been altered to titanite (Fig. 3d). Therefore, petrographic studies substantiate the potential role of post-magmatic alteration in modifying the mineralogy, although the texture and fabric remained largely unmodified after the crystallization of the mafic dykes.

The plagioclase laths had a low-angle relationship with the opaque grains. Their similarity in orientation is shown in photomicrographs of oriented thin sections cut along the magnetic foliation plane of the dyke samples (Fig. 4a–f). This can be considered a preliminary indication of the primary flow fabric. However, this interrelationship between the plagioclase and opaque grains has been further quantified through SPO analyses and discussed in greater detail in the subsequent sections.

4.c. Opaque Mineral Chemistry

The mineral chemistry study confirms that ilmenite and titanomagnetite are the dominant opaque phases in the studied mafic dyke samples.

4.c.1 Titanomagnetite

The raw data of the titanomagnetite were recalculated for Fe^{2+} and Fe^{3+} segregation based on its stoichiometry (Droop, 1987). The FeO and Fe_2O_3 contents of these grains range from 44 to 57 wt.% and 12 to 40 wt.%, respectively, and TiO_2 content lies between 15 and 28 wt.%. These grains show a distinct solid solution between magnetite and ulvöspinel in the FeO-Fe_2O_3-TiO_2 triangular diagram (Fig. 5). Furthermore, they also have some minor Al_2O_3, varying between 0.07 and 8 wt.% (Supplementary Table S2).

4.c.2. Ilmenite

The TiO_2 in the ilmenite grains varies from 49 to 50 wt.%, and their FeO content ranges from 40.5 to 44 wt.%. In addition, minor Fe_2O_3 and MnO were also recorded, which lie between 3 and 6 wt.% and 0.8 and 2.8 wt.%, respectively (Table S2). The Fe^{2+} and Fe^{3+} were stoichiometrically segregated during recalculation based on six oxygen atoms using an ilmenite recalculation sheet (© Gabbrosoft, 2012).

4.d. Anisotropy of magnetic susceptibility

4.d.1 Mafic Dykes

The mean AMS data from the 24 locations from both the sub-swarms of the studied ca. 2.21 Ga dyke swarm are compiled in
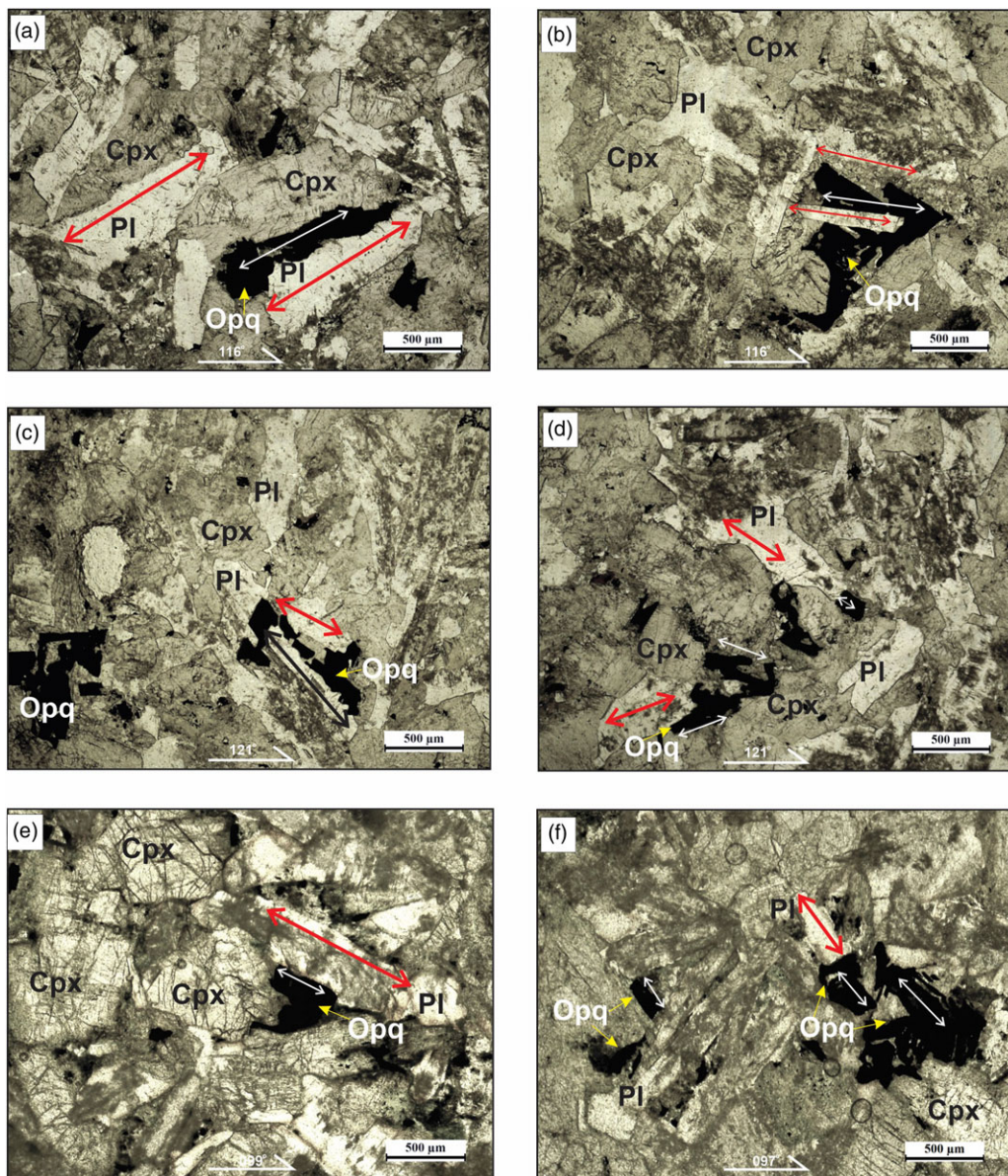
Figure 4. (Colour online) (a–f) PPL photographs of oriented thin sections from the two sub-swarms, for observing interrelationship between opaque and plagioclase fabric. The thin sections are cut along the K_1–K_2 planes of the samples, and the orientation of the horizontal image axis is marked at the bottom edge of the sample. (a) and (b) belong to EDC 21/4 (dyke 6 in Table 1a), (c) and (d) belong to EDC 20/32A (dyke 3 in Table 1a), (e) belongs to EDC 22/10a (dyke 18 in Table 1a) and (f) belongs to EDC 22/30B (dyke 20 in Table 1a). The opaque and plagioclase fabrics display distinct low angle relationships.
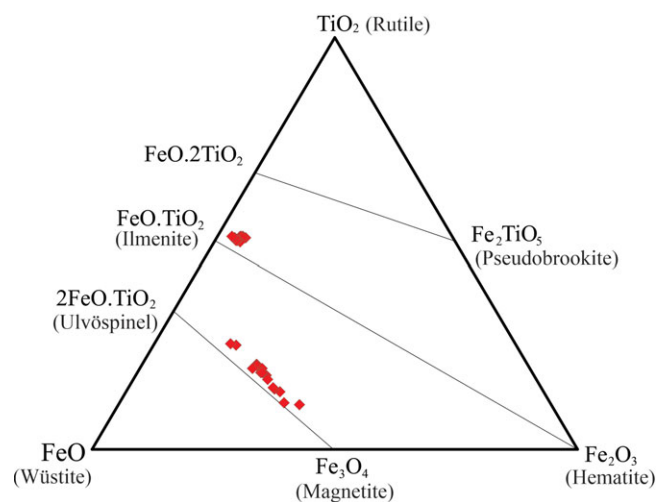
Figure 5. (Colour online) FeO – Fe$_2$O$_3$ – TiO$_2$ ternary diagram for classifying the Fe – Ti oxides observed in the samples. Mineral chemistry data were obtained from EPMA analyses.

Table 1a. The values of each individual core/cube specimens are further included in Supplementary Table S4. Dykes 1–16 (as mentioned in Table 1a and Fig. 1b) represent dykes from sub-swarm-1 exposed in the central part of the EDC, whereas dykes 17–24 (see Table 1a and Fig. 1b) are from sub-swarm-2, exposed in the northern part of EDC. The K_m values of the sub-swarm-1 range between 2023 and 59,260 μSI (see Table 1a), whereas the K_m values for the dykes from sub-swarm-2 vary between a relatively narrower range (1527–22720 μSI) (see Table 1a). The dominant population of bulk susceptibilities of the individual cores from sub-swarm-1 dykes is below 20000 μSI with a few outliers extending as high as 70000 μSI (Fig. 6a). Sub-swarm-2 has comparatively lower bulk susceptibility with a maximum population below 10000 μSI, where few higher outliers do exist but are restricted below 30000 μSI (Fig. 6b). Both the sub-swarm have sub-horizontal to inclined K_1 axes, where the K_1 inclination of the sub-swarm-1 dykes range from 1° to 55°, and the sub-swarm-2 dykes vary between 0° and 50°.

Undeformed mafic dykes generally show low degrees of Anisotropy (P_j) (e.g., Ernst & Baragar, 1992; Wiegand *et al.*
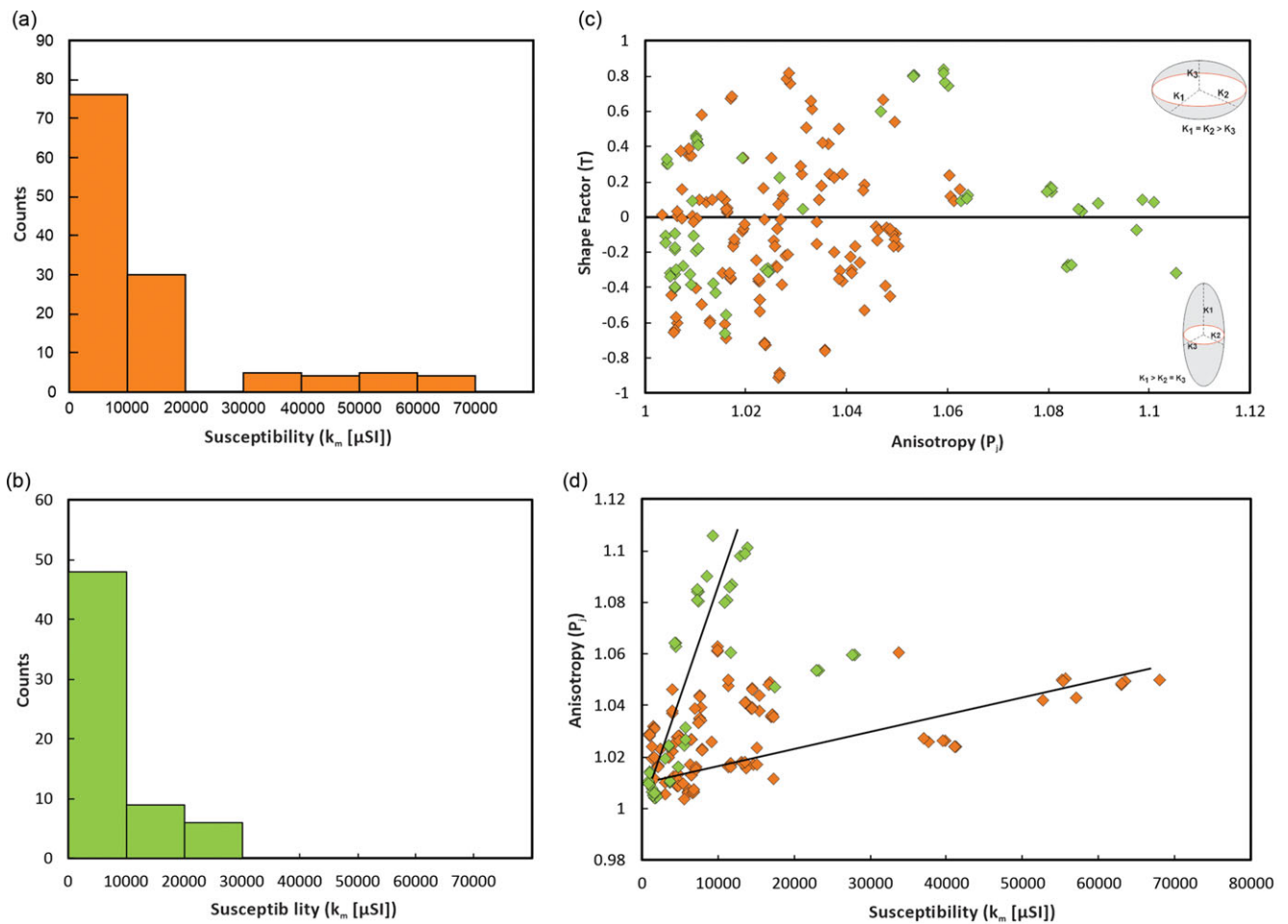
Figure 6. (Colour online) (a) Frequency distribution plot of bulk susceptibility (K_m) of the sub-swarm-1 dykes. (b) Frequency distribution plot of bulk susceptibility (K_m) of the sub-swarm-2 dykes. (c) P_j vs. shape parameter (T) after Jelinek, (1981) for all the studied dyke samples. (d) Bulk susceptibility (K_m) vs corrected degree of anisotropy (P_j) plot for all the dyke samples analysed. Black solid lines demarcate the approximate relationship between the K_m and P_j values. The orange markers denote specimens from sub-swarm-1 dykes and the green parkers represent specimens from sub-swarm-2 dykes.

2017), which is consistent with our results. The P_j values of the dykes from sub-swarm-1 and -2 vary from 1.009 to 1.048 and 1.005 to 1.087 (see Table 1a), respectively, and can be approximated as the representatives of primary fabrics (cf. Wiegand *et al.* 2017; Tarling & Hrouda, 1993). The shape parameter (T) for sub-swarm-1 lies between −0.6 and 0.5, whereas for sub-swarm-2, varies between −0.2 and 0.8 (see Table 1a). The dykes of the sub-swarm-1 are widespread over the prolate and the oblate zones of the Jelinek plot (Fig. 6c), with a slight dominance in the prolate zone. In the sub-swarm-2, dykes with lower P_j values preferentially have prolate fabrics, and those with higher P_j lie more or less in the neutral domain ($T = −0.2$ to $+0.2$), and only two dykes with low to moderate P_j lie in the oblate domain. The dykes from sub-swarm-1 display a more significant increase in K_m for a limited increase in P_j value, whereas the sub-swarm-2 dykes have a greater increase in P_j for a little increase in K_m (Fig. 6d). However, both the sub-swarms show a broad positive correlation between the P_j and K_m values (Fig. 6d), which can be interpreted as a basic mineralogical control over the increasing bulk susceptibility.

4.d.2 Host Granite

Host granites from five locations (i.e., 3, 10, 11, 12, and 24; see Fig. 1b) were collected, processed and analysed for AMS,

and the data are shown in Table 1b. The granite samples show K_m values ranging from 60 to 7570 μSI. The plunge of the K_1 axes offers an extensive range from 4° to 70°. The P_j values range from 1.04 to 1.2, indicating low to moderate degrees of anisotropies. The T values are dominantly positive (0.12–0.5), suggesting they might have undergone flattening strain.

4.e. Silicate fabric data

The SPO analyses of the four dykes – dykes 3 and 6 from sub-swarm-1 and dykes 18 and 20 from sub-swarm-2 (see Table 1a) – were conducted along their respective magnetic foliation planes. Dyke 3 has both the silicate and opaque fabrics mostly oriented along 081°–086° (Fig. 7). However, the plagioclase laths also have considerable population along 051°–056° (Fig. 7). The dominant orientation of the plagioclase grains for dyke 6 trended between 251° and 261° with substantial population along 231°–236° and 266°–271° (Fig. 7). The opaque mineral fabric of the dyke shows good correlation with the silicate mineral fabric, i.e. its dominant trend is along 266°–271° with a considerable population along 251°–256° and 261°–266° (Fig. 7). In sub-swarm-2, dyke 18 displays plagioclase fabric dominantly trending between 109°and 114° with considerable population along 254°–259° (Fig. 7).
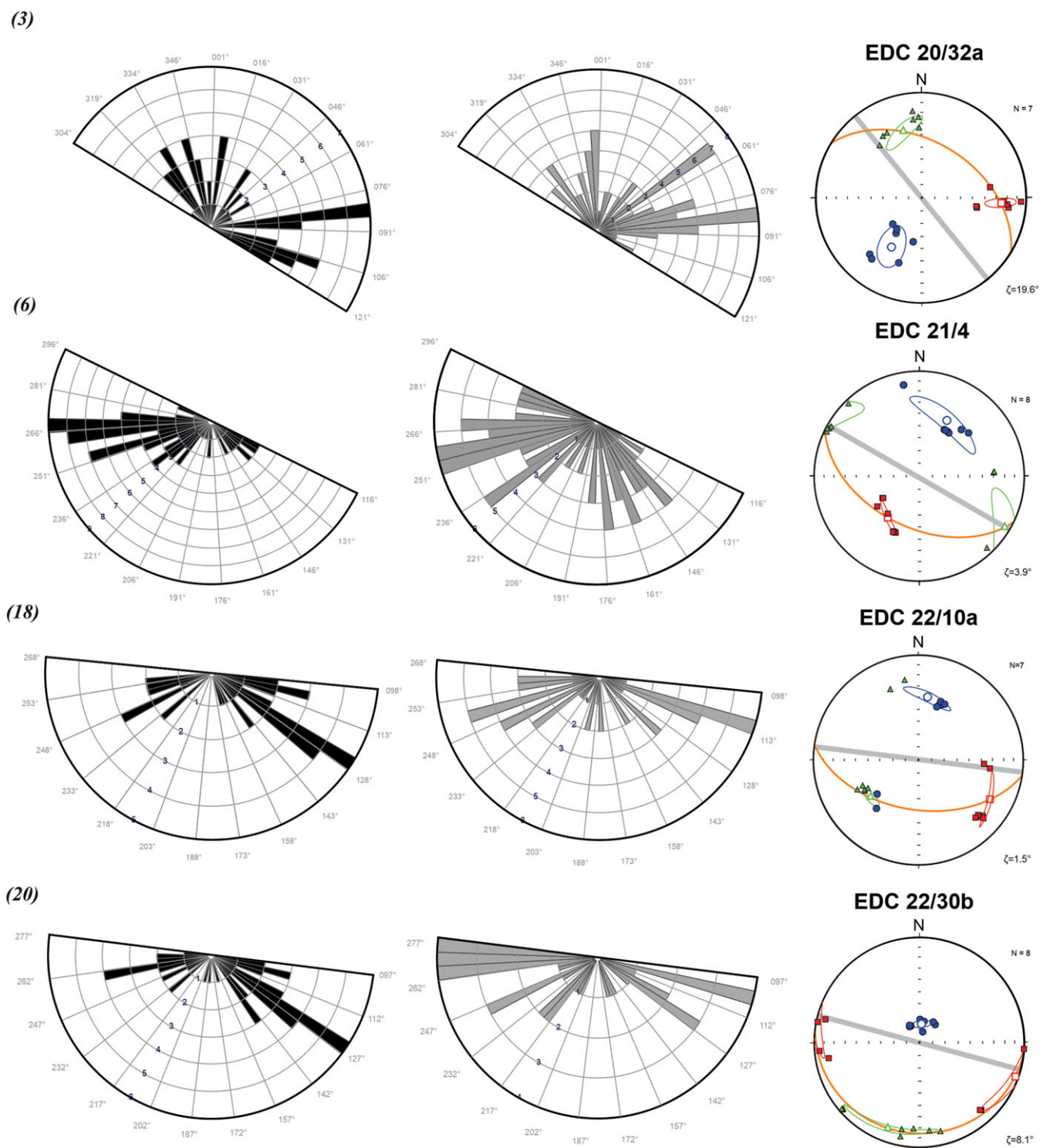
Figure 7. (Colour online) SPO analyses comparing the opaque fabric (rose diagram marked in black), plagioclase fabric (rose diagram marked in grey) and the respective magnetic anisotropy axes. The straight line of the semi-circular roses demarcates the orientation of the horizontal image axis, and the rake of the grains is measured in the rose diagrams.

The majority of the opaque grains trend along 124°–134° (Fig. 7). Dyke 20 has plagioclase grains trending along 102°–106° and 262°–277°, and the opaques are oriented along 122°–127° (Fig. 7). All the dykes show good correlation between the opaque fabrics, plagioclase fabrics and are also consistent with the respective magnetic lineations.

5. Discussion

5.a. Evidence from Magnetic Anisotropy data

5.a.1. Mafic Dykes

The mafic dykes display high bulk magnetic susceptibilities (1527–59260 µSI), which is indicative of the dominance of

ferro/ferri-magnetic mineralogy (e.g., Knight & Walker, 1988; Hargraves *et al.* 1991; Rochette *et al.* 1992). Their magnetic fabric is primarily due to the shape anisotropy of titanomagnetites. The oxide grains in the dykes show a solid solution between ulvöspinel and magnetite (Fig. 5), and the opaque mineral chemistry is not significantly different between the sub-swarms. Ulvöspinel is paramagnetic at room temperatures (Moskowitz *et al.* 2015) and, thus, will not affect the direction of anisotropy due to titanomagnetite grains. The exsolved ilmenite lamellae are moreover antiferromagnetic at room temperature (Lowrie & Fichtner, 2020), making them ineffective at controlling the induced susceptibilities. As a result, titanomagnetite is the only grain with the ability to produce such high K_m values.

Although both the sub-swarms have magnetic susceptibilities in the ferro/ferri-magnetic domain, dykes of the sub-swarm-1, however, show higher K_m values as compared to the sub-swarm-2 (Fig. 6a, b). Given that the K_m value roughly corresponds to three times the volume of magnetite in a sample (Mooney & Bleifuss, 1953) and that there are no obvious differences in the mineral chemistry of the magnetic grains, it is reasonable to assume that the higher K_m values for some of the dykes in the sub-swarm-1 are the result of a higher Ti-magnetite grain concentration. On the contrary, the dykes of sub-swarm-2 display a greater variance in their P_j values as compared to the K_m values (Fig. 6d), which suggests the titanomagnetites have variation in grain shape, i.e. from isotropic to moderately elongated (anisotropic). This is possible by the Ti-magnetite crystallizing in a bimodal manner, with the earlier crystals being more isotropic and the later crystals being more anisotropic due to rapid cooling. Moreover, as mentioned earlier, some of the opaque grains have been altered to titanite, this might also be a possible cause for reducing the bulk magnetic susceptibility in some of the studied dykes.

The principal anisotropy axes and the mean axes for the studied dyke samples were plotted on lower hemisphere equal-area stereographic projections. Wherein the foliation plains were marked, and the angle between the K_1-K_2 plane and the dyke plane, denoted by ζ (zeta), was calculated by overlaying them with the field measurements of the dyke planes (Fig. 8). The observed magnetic fabrics are classified into three groups, viz. subparallel, oblique and perpendicular. Ideally, the imbrication of the magnetic foliation plane (K_1-K_2) and the orientation of the magnetic lineation (K_1) are considered to identify the nature of the fabric in the case of oblate and prolate samples, respectively (Geoffroy *et al.* 2002; Das *et al.* 2021). However, as the samples are relatively weakly anisotropic, we considered ζ as the characteristic factor for all the samples. Multiple field observations of the road cut (Fig. 2b–d) and canal cut sections suggest the dyke planes to be more or less vertical. The same has been considered in the AMS stereoplots (Fig. 8) while comparing them with the magnetic foliation planes. The classification mentioned above is further discussed as follows:

(i) Subparallel fabric: We consider the dyke samples with ζ <25° to demonstrate subparallel fabric (cf. Ernst & Baragar, 1992; Das *et al.* 2021). This fabric is evident from 8 out of 16 (50%) of the dyke samples of sub-swarm-1 (see dykes 1–8 in Table 1a and Fig. 8a) and 5 out of 8 samples (62.5%) of sub-swarm-2 (see dykes 17–21 in Table 1a and Fig. 8b). The magnetic lineations for both the groups are sub-horizontal and inclined (3°–48°). The ellipsoid shape (T) ranges from prolate through neutral to oblate domains for the sub-swarm-1, with a dominance of neutral ellipsoids (see Table 1a), whereas the subparallel fabric dykes of sub-swarm-2 have mainly neutral to oblate ellipsoids, with the more anisotropic samples preferentially showing planar (oblate) fabrics (see Table 1a).

(ii) Oblique fabric: The samples with ζ lying between 25° and 45° are included in this group. Five dyke samples from sub-swarm-1 (dykes 9–13 in Table 1a and Fig. 8a) and one dyke from sub-swarm-2 (dyke 22 Table 1a and Fig 8b) show such fabric. All the K_1 axes in this group are sub-horizontal to inclined (1°–55°). Furthermore, all the dykes from this group displayed neutral ellipsoids, except one (dyke 9) which has prolate magnetic ellipsoid (see Table 1a).

(iii) Perpendicular fabric: This fabric is represented by three dyke samples of sub-swarm-1(dykes 14–16 in Table 1a and Fig. 8a) and two samples of sub-swarm-2 (dykes 23 and 24 in Table 1a and Fig. 7b), which have high values of ζ (46°–90°). The former samples have moderately plunged K_1 axis lying between 15° and 46°, whereas the latter display sub-horizontal K_1 axis plunges (<10°). The anisotropy ellipsoids of both trends have weakly negative T values, indicating their neutral ellipsoidal shapes (see Table 1a).

When all the dykes are considered together, we observe a dominance of T lying between −0.2 and +0.2 for both the sub-swarms, which suggests neutral ellipsoidal shapes for the studied samples. However, this may also be an indication that both planar and linear fabrics have contributed to the magnetic anisotropy. As magmatically generated fabrics are more random compared to deformation fabrics, the latter reason, i.e. involvement of both planner and linear grains in the magnetic anisotropy, seems more reasonable. Further, in the P_j vs. K_m plot (Fig. 6d), the dykes display a broad positive correlation between the anisotropy and bulk susceptibilities, suggesting that the magnetic anisotropy increased with the increase in bulk susceptibilities. Fig. 6c and 6d shows a mineralogical control over the magnetic anisotropy for both the sub-swarms.

The good geometric correlation between silicate and opaque fabric orientations in mafic dyke samples, as observed by petrographic inspection of oriented thin sections (Fig. 4a–f), indicates that the magnetic fabric essentially mimics the silicate flow fabric. Therefore, the effects of size-related domain structure (single, multi- and pseudo-single domain) of the magnetites on the observed magnetic anisotropy are considered non-critical (Sen & Mamtani, 2006; Archanjo *et al.* 1995) for the present work. However, SPO analyses were conducted to further validate the interrelationship between silicate and magnetic fabric.

5.a.2. Petrofabric of mafic dykes

The reliability of AMS data as prospective magma flow indicators must be confirmed because it is susceptible to post-magmatic reorientation and frequently shows composite fabrics. SPO analyses present an effective method to substantiate the relationship between the magnetic and the silicate flow fabrics and validate the usability of the AMS data for deciphering magma flow. Figure 7 demonstrates the results of SPO analyses of four mafic dyke samples with subparallel magnetic fabrics. They display a good comparison between the opaque and the silicate fabrics measured in the magnetic foliation plane. This suggests that the preferred orientation of the magnetic carrier minerals (opaque grains) is indeed related to the primary magma flow. Further, the dominant orientation in the opaque rose diagrams has a good correlation
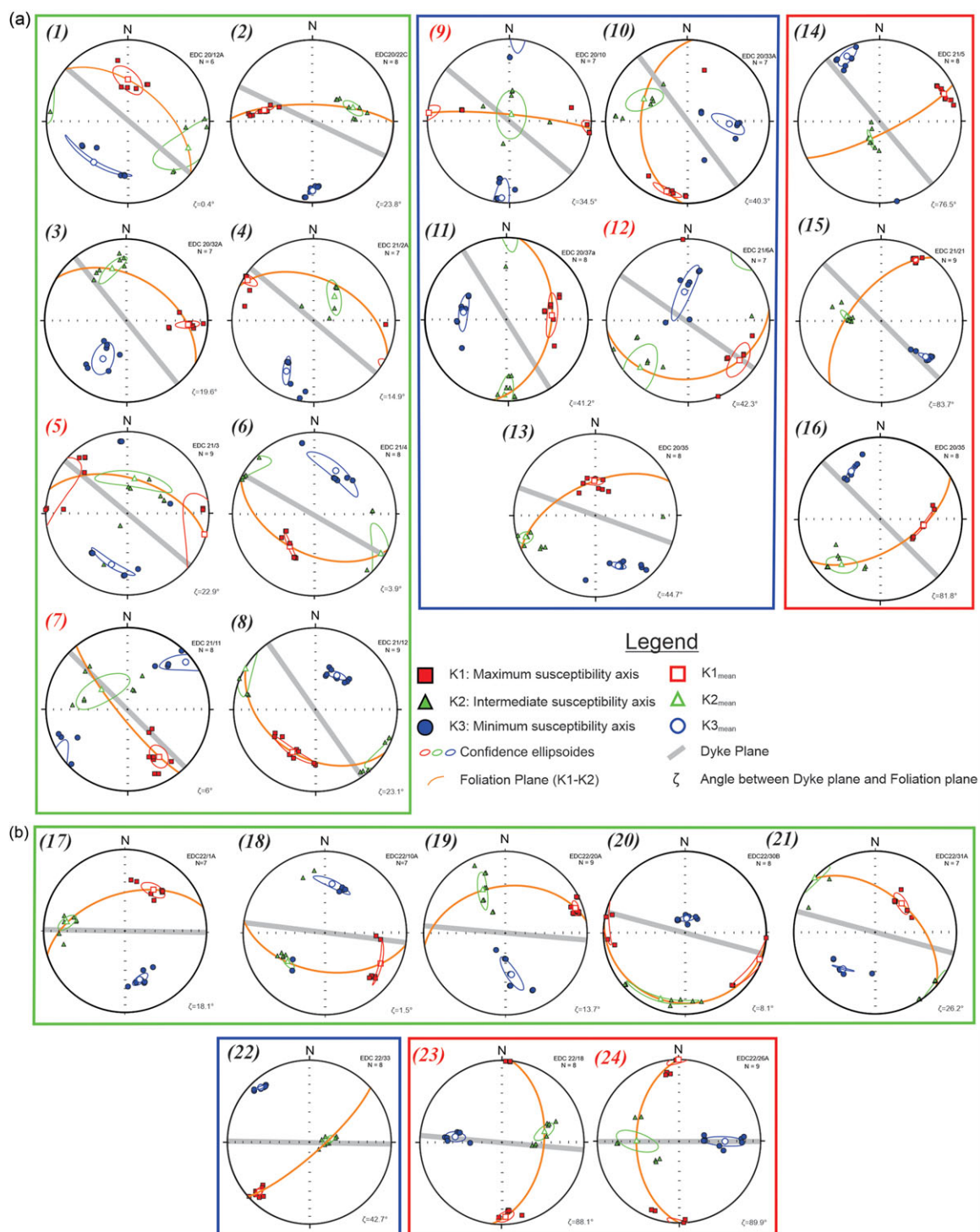
Figure 8. (Colour online) (a) Lower hemisphere equal area projections of eigen vectors K_1 (red squares), K_2 (green triangle) and K_3 (blue squares) for the studied NW-trending ca. 2.21 Ga dyke swarm mafic dykes from in and around Anantapur district, Andhra Pradesh. (b) Lower hemisphere equal area projections of eigen vectors K_1 (red squares), K_2 (green triangle) and K_3 (blue squares) for the studied E-trending ca. 2.21 Ga dyke swarm mafic dykes from in and around Hyderabad district, Telangana. The 95 % confidence ellipsoids could be constructed for samples with at least five cylindrical core or cube specimens. The Magnetic foliation plane is marked as an orange great circle. The dyke plane is marked as the thick grey line. The samples are categorized into three groups viz. subparallel (green demarcation), oblique (blue demarcation) and perpendicular (red demarcation). The serial numbers are the same as those used in Table 1a.

with the respective magnetic lineation (K_1 axis orientation), indicating that the observed magnetic anisotropy is a product of the shape anisotropy of titanomagnetites. This substantiates our assertion that the magnetic anisotropy holds a relationship with the SPO of the opaque grains, and there are no discernible changes in the anisotropy due to the effect of the size-dependent domain structure of magnetite. From the detailed SPO analyses, we further confirm that the AMS fabric of the mafic dyke samples is a product of primary magma flow and, therefore, can be successfully used as a proxy to study the magma flow dynamics.

The preferred orientation of asymmetric ferromagnetic grains in mafic dyke samples reflects the observed magnetic anisotropy (Nagaraju & Parashuramulu, 2019). Generally, however, there are two approaches to interpreting magma flow dynamics using AMS data: the first approach involves the interpretation of only the subparallel magnetic fabrics to formulate geologically meaningful information about magma flow dynamics, whereas the second approach considers the anomalous fabrics (oblique and perpendicular) to identify any flow related or secondary event, which might have generated these fabrics and helps to avoid misinterpretations. In the presented dataset, a sizeable number of samples display anomalous magnetic fabrics. Herein, we have provided suitable rationales for these fabrics before interpreting the samples having subparallel fabric, to attain a better-filtered understanding of the magma flow dynamics within these dykes.

(i) Anomalous Fabrics

In the presented dataset, 11 out of 24 mafic dyke samples display anomalous magnetic fabrics. Their considerable population has the potential to influence the larger dataset, which might, in turn, lead to several misinterpretations regarding magma flow dynamics. Both field observations and satellite imagery are considered to interpret these observed fabrics; these include – (i) dyke 12 (see Table 1a and Fig. 8a) displays oblique fabric with easterly trending, shallowly dipping magnetic foliation (Table 1a). During fieldwork, several fracture sets ranging from 050° to 135° in the dolerite and the country rock exposures in the vicinity were observed. This indicates a later fracturing event (cogenetic or unrelated) that might have reoriented the magnetic fabrics in a quasi-solid state; (ii) dyke 13 from sub-swarm-1 (see Table 1a and Fig. 8a) in the central EDC and three dykes in sub-swarm-2, i.e. dykes 22, 23 and 24, respectively (see Table 1a and Fig. 8b) in the northern EDC display anomalous fabrics, which might be attributed to the reorientation of magnetic carrier minerals in response to the emplacement of younger ca. 2.08 Ga dykes in the vicinity (Fig. 1a); (iii) Further, dyke 15 (see Table 1a and Fig. 8a) displays NE-trending magnetic foliation, which holds an orthogonal relationship with the dyke plane. Using satellite imagery, a NE-trending lineament is identified in the vicinity, which is inferred to be a dextral shear that formed after the emplacement of the ca. 2.21 Ga dyke swarm, as it displaces the dyke exposures on either side of it (Figs. 1b and 10c). However, evidence for such a shear zone could not be observed in the field due to dense foliage cover and (iv) dykes 9, 10 and 11 (see Table 1a, and Fig. 8a) display ζ around 36° (Table 1a), which is attributed to the imbrication angle formed by platy grains with the dyke wall in a dynamic magma system (Knight & Walker, 1988).

(ii) Subparallel Fabrics

After filtering the anomalous fabrics, the dykes with subparallel magnetic fabric and those with oblique fabric related to imbrication with the dyke wall (dykes 9, 10 and 11 in Table 1a) are considered for interpreting the broad magma flow direction following the conventional approach (Raposo & Ernesto, 1995). The K_1 axes of these dykes have sub-horizontal to moderate plunges, which suffice for lateral and inclined magma flow (*discussed later in detail*) within the dyke fractures.

5.a.3. Host Granites

The Dharwar Craton crust stabilized ~200 Myr before the emplacement of these dykes, and all large-scale deformation events of the craton pre-date the dyking events (e.g., Drury *et al.* 1984; Chadwick *et al.* 1989; Jayananda & Mahabaleswar, 1991; Bouhallier *et al.* 1993). Moreover, no significant regional deformation event has been recorded after (or during) the emplacement of the Paleoproterozoic mafic dyke swarms. Although earlier workers have suggested large-scale oroclinal bending, leading to anticlockwise rotation of the northern part of the Dharwar Craton during the Paleoproterozoic (before ca. 2.08 Ga) (Söderlund *et al.* 2019), such a large-scale rotation would result in extensive oceanic spreading, lithospheric thinning and rift-related magmatism along the rotation axis (Söderlund *et al.* 2019). Such evidence is largely absent in the case of Dharwar Craton. Moreover, such large-scale anticlockwise rotation would have considerable compression along NW in the northern part of the craton, which would have conspicuous imprints on the country rock. We could not find supporting evidence for the rotation of the Dharwar Craton in our petrofabric inspections of the host-granitoid. However, as our dataset for the host granitoids was relatively less in number, and our main focus was on the mafic dyke samples, it would be speculative to confirm or reject the possibility of the oroclinal bending in the Dharwar Craton.

It is, therefore, reasonable to consider that the present-day structural grain of the host granitoids developed much before the dyke emplacement and had the potential to influence the dyke emplacement systems. The AMS analyses of the host granites were conducted to study the structural fabric of the country rock. The measured K_1-K_2 planes were compared with the dyke trends (Fig. 9) and the geometry of the repeating fracture sets in the area (Fig. 9), which allowed us to inspect the relation between the pre-existing structural grain of the country rock and the primary magmatic stress field of the studied dykes.

The granites can be classified into three groups based on their K_1-K_2 planes:

(i) Granites from locations 10, 12 and 24 (see in Fig. 1b), i.e. samples EDC 20/33B, EDC 21/6B and EDC 22/6B in Table 1b, have their K_1-K_2 planes trending subparallel to the dyke plane (Fig. 9) and the intra-terrane shear zones (Fig. 1b) in the area. Further, both the dyke geometry and the magnetic foliation of the host granites show a good correlation with the dominant trends of the fracture sets (WNW to NW) (Fig. 9). This indicates a complementary relationship between the structural grain of the country rock and the magmatic stress field of the dyke swarm. Similar suggestions were made by Datta *et al.* (2023) based on their statistical analyses.

(ii) The second category includes a sample from location 3 (see in Fig. 1b), i.e. EDC 20/32B in Table 1b, that lies between two NW-trending intra-terrane shear zones. The foliation plane demonstrated by this sample makes an angle of 41° with the intra-terrane shear zones and 37° with the dyke plane (Fig. 1b, 9), indicating a complex relationship between the dyke geometry and the structural fabric of the host granitoids.

(iii) The third category includes a sample from location 11 (see in Fig. 1b), i.e. EDC 20/37B in Table 1b. This granite shows an orthogonal relationship of the magnetic foliation plane with the intra-terrane shear zones and dyke trends (Fig. 1b, 9). This location lies in the vicinity of an intersection between NW-trending ca. 2.21 Ga dyke and ca. 2.08 Ga NE-trending younger dyke. AMS data record the last stage deformation in a rock; therefore, it is reasonable to
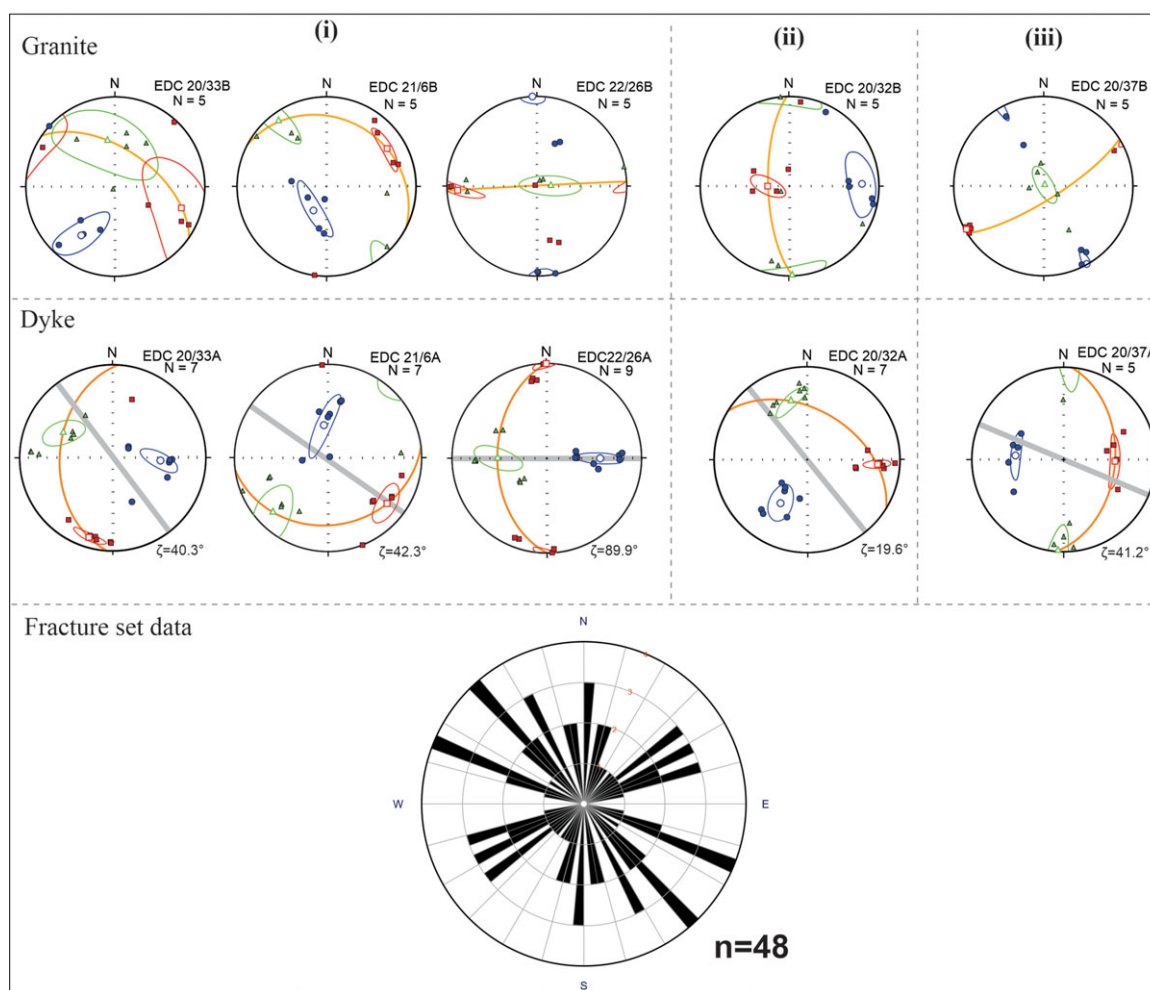
Figure 9. (Colour online) Lower hemisphere equal area projection of magnetic eigen vectors for the host granitoid. They are compared with the plots for the associated mafic dyke samples. The symbols for the susceptibility axes are the same as in Fig. 8. Further, the magnetic fabrics of the mafic dykes and associated host granites are correlated with the rose diagram of the repetitive fracture sets measured in the field, 'n' represents the number of fracture sets measured.

consider the magnetic foliation plane of this location to be an artefact of the influence of NE-trending younger dyke intrusion rather than the regional paleostress field.

All the granite samples except one (i.e., EDC 20/37B; location 11 in Table 1b) display positive T values. This indicates oblate susceptibility ellipsoid, which suggests the influence of a compressive stress regime related to regional transpression (cf. Fossen, 2016). This stress regime can be related to the much older transpressive convergence of the EDC and the WDC (cf. Chardon et al. 2008). Additionally, the granite sample exhibiting prolate susceptibility ellipsoid (location 11 in Fig. 1b) displays a sub-horizontal K_1 axis-trending along NE, and the magnetic foliation plane is subparallel to the NE-trending younger (ca. 2.08 Ga) dyke in the vicinity. Therefore, the observed magnetic fabric in this granite sample may be due to the compression imposed on the adjacent country rock in response to the emplacement of the younger dyke. This compression would be at high angle to the NE-trending dyke, which subsequently resulted in the axially symmetric extension (cf. Fossen, 2016) of the magnetic markers (and other grains) in the adjacent country rock along the NE direction.

5.a.4. Plume centre location and magma flow dynamics

As the NW- and WNW-trending dykes belong to the two sub-swarms of the ca. 2.21 Ga Anantapur–Kunigal dyke swarm, its spatial span suggested a southeasterly opening with a fanning angle of ~35°. Based on the geometry of the dyke swarm, its convergence to a focal point towards the NW of the present Dharwar Craton (cf. Yadav et al. 2020), at a distance of about 630 km from our sampling locations in the central part of EDC and about 610 km from our sampling locations in the northern part of EDC, is suggested (Fig. 10a). As discussed earlier, with the present AMS dataset of dykes along with structural grain of host granite, it is challenging to ascertain the potential rotation between north and south Dharwar Craton as suggested by Söderlund et al. (2019). Therefore, the current proposal regarding the location of the plume centre does not consider the rotation model of the Dharwar Craton. In the present work, the location of the plume centre is established solely based on the present-day geometry and the dyke density. To precisely constrain the location of the plume centre, more detailed paleomagnetic studies and margin-to-margin AMS inspection of several dykes are required. In the present work, as the distinct dyke margins were lacking, profiling the entire dyke widths was difficult.
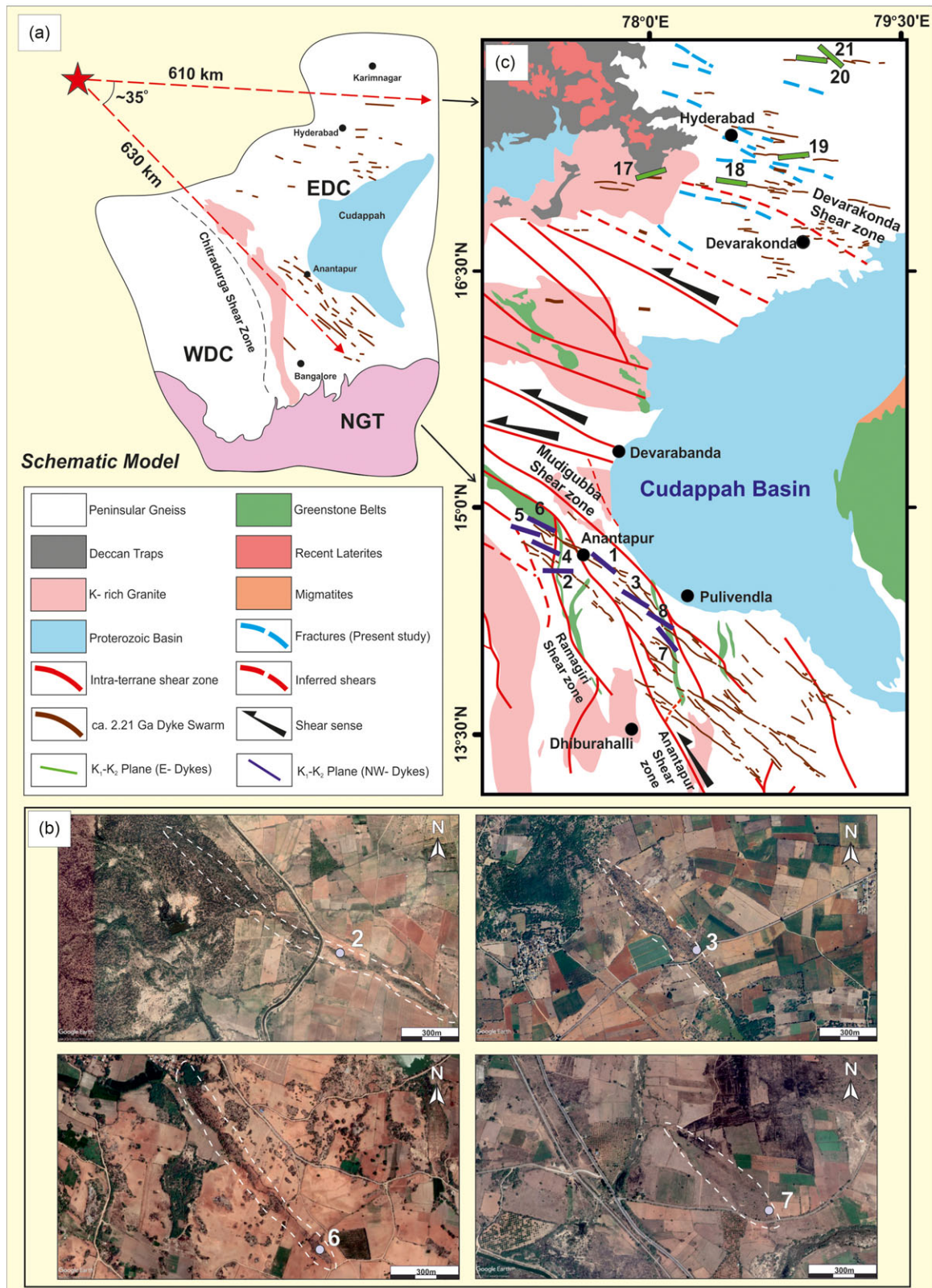
Figure 10. (Colour online) (a) Schematic model of possible plume for ca. 2.21 Ga Anantapur–Kunigal swarm (after Samal *et al.* 2021b). (b) Satellite imagery of sampling locations denoting the distal location of some representative samples that displayed plunging K_1 axes. (c) The magnetic foliation plane (K_1–K_2) for the dyke samples with subparallel fabric is plotted in the study area map (after Chardon *et al.* 2008; French and Heaman, 2010) for comparison with the intra-terrane shear zones and fractures in the country rock.

This restrained studying the imbrication relationship of magnetic carrier minerals in the opposite chilled margins.

In our presented dataset, 13 mafic dykes with subparallel magnetic fabric and 3 of the oblique fabric dykes (dykes 9 10, and 11 in Table 1a), which were attributed to the imbrication of magnetic minerals, were used to study the magma flow dynamics. Out of these selected dykes, 50% of the data display sub-horizontal magnetic lineation, and the other 50% display moderately plunging magnetic lineation. The sub-horizontal K_1 axes can be related to possible lateral magma flow from the distantly located plume centre. This mechanism is also supported by several other worldwide studies, wherein lateral magma flow is reported at distances greater than 500 km from the plume centre (e.g., Ernst & Baragar, 1992; Hou *et al.* 2006; Ramesh *et al.* 2020). However, the considerable number of dykes with plunging magnetic lineation needed special attention. The majority of the samples that showed plunging K_1 axes were collected from the distal end of the dyke segments, i.e., towards SE in the sub-swarm-1 dykes and towards E in the sub-swarm-2 dykes, as verified from Google^{TM} Earth imagery (Fig. 10b). This relation can be an indication for a possible inclined magma movement at the distal end of the dyke fractures. A similar magma emplacement model has been suggested on a local scale, based on field observation and the interrelationship between pre-existent joints and *en-echelon* dyke fragments by Healy *et al.* (2018). In the present work, we suggest a similar type of magma emplacement for some of the dyke fragments, which are spread across the entire study area.

5.b. Constraints from magnetic foliation data

The K_1-K_2 planes of dyke samples representing subparallel fabric were plotted on the study area map to compare them with the dyke trends and the intra-terrane shear zones (Fig. 10c). The mafic dykes of the sub-swarm-1 primarily lie close to the NW-trending Anantapur shear zone, Mudigubba shear zone and locally N-trending Ramagiri fault (Fig. 10c), and the sub-swarm-2 samples lie in the vicinity of several east-trending intra-terrane shear zones inferred from our field evidence (Fig. 10c). These samples were further classified into three groups based on their relationship with the adjacent shear zones: (a) the magnetic foliation plane displayed by five dykes (dykes 1, 3, 4, 5 and 6 in Table 1a) lies subparallel to the Anantapur shear zone and the dyke planes (Fig. 10c). Consequently, the dykes from the sub-swarm-2 (dyke 18–19 in Table 1a) from the northern part of EDC have a subparallel relationship with the Devarakonda shear zone and associated E-trending fractures (Fig. 10c); (b) two dykes (dykes 7 and 8 in Table 1a) lie close to the Mudigubba shear zone having low angle relationship with the dyke plane and the shear zone (Fig. 10c) and (c) one dyke (dyke 2 in Table 1a) lying close to the Ramagiri fault, with its magnetic foliation plane having an orthogonal relationship with the adjacent shear zone but a low angular relationship with the dyke plane. This might reflect the dominance of primary magma flow over the pre-existing stress regime. From the above observations, we infer that the magmatic stress regime of the Anantapur–Kunigal dyke swarm was broadly complemented by the imprints of the pre-existing regime of the country rock during its emplacement, and wherever the relationship was not constructive (dyke 2 in Fig. 10c), the magmatic stress regime dominated. Further, the low-angle relationship between the magnetic fabric of the country rock, the dyke orientations and the orientation of the crustal inhomogeneities suggests the structural grain of the country rock has supported the original radiating

pattern of the dyke swarm. This further implies that this supportive scenario resulted in primary lateral dyke propagation subparallel to the structural grain of the country rock. During the process, it is reasonable for the magma to have also injected into the pre-existing weak planes of favourable geometry present in the EDC crust and employ them as potential pathways for magma transport. Considering our inferences, we formulated an emplacement model for the studied dyke swarm that is discussed below.

5.c. Emplacement model for the studied dyke swarm

The Neoarchean convergence of the EDC and WDC is well established (Jayananda *et al.* 2018; 2020; and references therein); however, the dynamics of this event are still under debate. The earlier researchers have proposed several models that support the subduction-accretion theory (e.g., Drury *et al.* 1984; Chadwick *et al.* 2007; Jayananda *et al.* 2013; Rao *et al.* 2015; among others) or plume tectonics theory (e.g., Bouhallier, 1994; Chardon, 1997; Jayananda *et al.* 2000), or combination of both plate- and plume tectonics (e.g., Chardon *et al.* 1998; Harish, 2003; Manikyamba & Kerrich, 2012). Based on desktop and field observations, Chardon *et al.* (2008) suggested lateral flow of the weaker lithosphere of the EDC against the stronger WDC core. This crustal channel flow and oblique transpressive accretion were accommodated by NW- to NE-trending intra-terrane shear zones in the EDC (Fig. 1b, b). Further, based on structural and field evidences, these intra-terrane shear zones were modelled as listric and dipping towards the northeast, with an inferred décollement at the Moho (Chadwick *et al.* 2007). Recent deep seismic studies of Rao *et al.* (2015) and Mandal *et al.* (2018) also confirm NE-dipping listric shears in the upper-middle crust of the EDC and have been related to the Neoarchean accretion event. Our magnetic anisotropy data of all the host granitoids furnished oblate ellipsoids and fit well in the transpressive oblique accretion model (cf. Chardon *et al.* 2008) of the EDC-WDC amalgamation. This implies that the granites have dominantly preserved a much older fabric induced by regional transpression due to deformation by flattening during the oblique Dharwar Craton accretion. The responsive structural grain represents the last-stage strain regime in the EDC crust, into which the studied dyke swarm might have been emplaced.

Based on our inferences and the abovementioned background, our emplacement model suggests that the ca. 2.21 Ga Anantapur–Kunigal dyke swarm was fed from a distant plume, from where the magma was injected laterally below the EDC. Further, some of the dykes were emplaced via lateral dyke propagation and sub-horizontal magma flow, whereas some others subsequently took up an inclined flow direction, which was especially observed at the distal ends of the dyke exposures (Fig. 11). The explicit parallelism of the pre-existing intra-terrane shear zones, fracture set geometry, dyke trends and the trends of the magnetic foliation of host granitoid, indicates that the emplacement of the dyke swarm was controlled mainly by the pre-existing structural grain of the country rock, which facilitated lateral dyke propagation in the EDC crust. In the process, the magma injected into several pre-existing crustal inhomogeneities that had a favourable geometry with respect to the location of the plume centre (Fig. 11). We further confirm, based on our emplacement model, that, on a broader scale, the imprints of the pre-existing regional stress field typically control the dyke emplacement, with the magmatic stress regime only having a minimal influence. However, when the available inhomogeneities are not conducive to magma transport, even at great distances from the plume centre, the primary magmatic stress
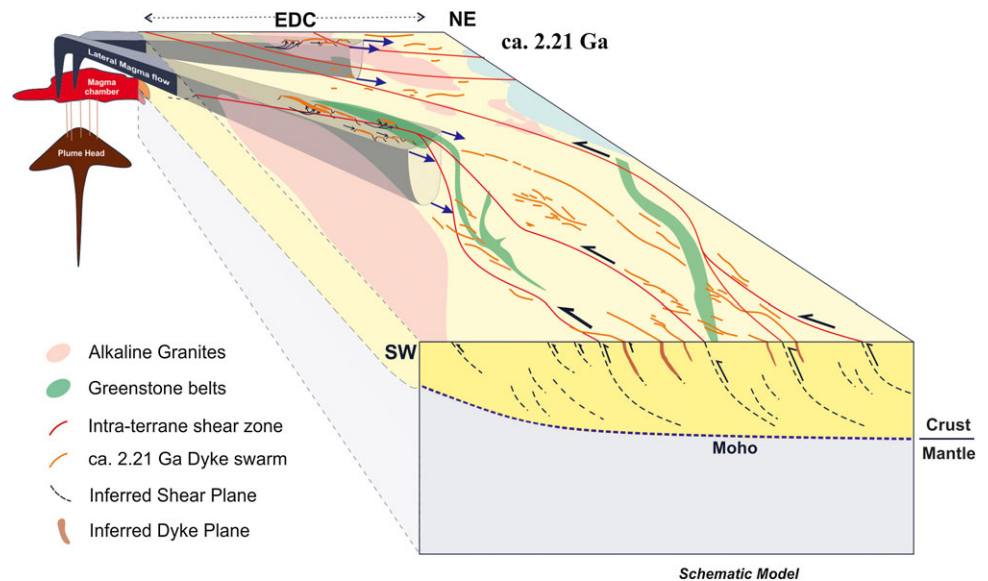
Figure 11. (Colour online) Schematic emplacement model for ca. 2.21 Ga Anantapur–Kunigal dyke swarm in a regional shear architecture after Chadwick *et al.* (2007) and Chardon *et al.* (2008).

will take control of the dyke emplacement by forming primary dyke fractures, provided there is sufficient magma input (dyke 2 in Fig. 10c).

6. Conclusions

a. The bulk magnetic susceptibility and mineral chemistry data suggest that the magnetic anisotropy observed in the mafic dyke samples of both the sub-swarms of the ca. 2.21 Ga Anantapur–Kunigal mafic dyke swarm of the Dharwar Craton is primarily controlled by the shape anisotropy of ferrimagnetic titanomagnetites.

b. The more considerable variance in K_m relative to the P_j values in sub-swarm-1 dykes suggests a greater concentration of titanomagnetites in some of the samples. A more significant variation in P_j as compared to K_m values in the sub-swarm-2 dykes indicates the presence of both isotropic and anisotropic Ti-magnetite grains in these dyke samples, plausibly due to multiple generations of oxide crystallization.

c. The predominance of neutral T values (-0.2 to $+0.2$) in both the sub-swarms indicates both planar and linear fabrics have contributed to the magnetic anisotropy. Further, a broad positive correlation between the P_j and T values suggests a primary mineralogical control on the observed magnetic anisotropy.

d. The excellent correlation in the three-fold comparison between the opaque fabric, silicate fabric and the magnetic lineation, observed in the SPO analyses in several oriented thin sections from the subparallel fabric samples, further validates the primary nature of the observed magnetic anisotropy and thereby established the AMS data as a reliable flow indicator for the studied dyke samples.

e. The sub-horizontal to plunging K_1 axes of the studied dyke samples indicates lateral magma flow from a spatially distant mantle plume, with some dykes showing inclined magma flow, especially at the distal end of the dyke fractures. The present-day geometry of the dyke swarm defines the location of the possible plume centre towards the NW of the Dharwar Craton, at a distance exceeding 610 km from the sample locations.

f. The oblate susceptibility ellipsoids for the host granite samples indicate the imprints of flattening deformation due to regional transpression related to the Neoarchean EDC-WDC convergence.

g. Based on the fitting correlation between the dyke geometries, intra-terrane shear zones, fracture set orientation and magnetic fabric of the country rock, we suggest the structural grain of the host rock, to have largely influenced the geometry of the studied dyke swarm. However, the magmatic stress regime took control of the dyke emplacement, by forming primary dyke fractures, in areas where the relationship between the pre-existing strain fabric and the magmatic stress was unfavourable. Otherwise, the magma propagated laterally for great distances through pre-existing subparallel inhomogeneities (shears and fractures) as well as by opening its primary dyke fractures. This supports our hypothesis that the original radiative nature of the dyke swarm was broadly complemented by the ambient regional paleostress regime. After this lateral flow, the magma in some dyke segments underwent subsequent inclined flow, which was observed especially at the distal ends of the dyke exposures.

CRediT authorship contribution statement. Srinjoy Datta: Investigation, data curation, formal analysis, methodology, visualization and writing – original draft.

Amiya K. Samal: Conceptualization, supervision, investigation, methodology, data curation, writing – editing and revision and fund acquisition.

Sayandeep Banerjee: Conceptualization, supervision, investigation, methodology, data curation, formal analysis, visualization, writing – original draft and revision and fund acquisition.

Rajesh K. Srivastava: Project administration, supervision, resources, writing – editing and fund acquisition.

Competing interests. The authors declare that they have no known competing financial interests or personal relationships that could have appeared to influence the work reported in this paper.

References

Archanjo CJ, Launeau P and Bouchez JL (1995) Magnetic fabric vs. magnetite and biotite shape fabrics of the magnetite-bearing granite pluton of Gameleiras (Northeast Brazil). *Physics of Earth and Planetary Interiors* **89**, 63–75.

Banerjee S, Maity S, Sarkar G and Acharya S (2022) The origin and localization of "vermiculite" along the intra-terrane shear zones in the Bundelkhand Craton, India: mechanism and implication. *Geological Journal* **57**, 3973–87.

Bleeker W and Ernst R (2006) Short-lived mantle generated magmatic events and their dyke swarms: the key unlocking Earth's paleogeographic record back to 2.6 Ga. In *Dyke Swarms—Time Markers of Crustal Evolution* (eds E Hanski, J Vuollo, S Mertanen and T Rämö), pp. 3–26. London: Taylor and Francis Group.

Borradaile GJ (1991) Correlation of strain with anisotropy of magnetic susceptibility (AMS). *Pure and Applied Geophysics* **135**, 15–29.

Bouhallier H (1994) Evolution structurale et metamorphic de la croute continentale arche´enne (Craton de Dharwar Inde du Sud). *Me´m. Doc., Ge´osciences Rennes* **60**, 277.

Bouhallier H, Choukroune P and Ballèvre M (1993) Diapirism, bulk homogeneous shortening and transcurrent shearing in the Archaean Dharwar Craton: the Holenarsipur area, southern India. *Precambrian Research* **63**, 43–58.

Cadman AC, Harris D and Ryan B (1993) An investigation of some metamorphosed mafic dykes of the Nain area, Labrador, Part 1. *Current Research. Geological Survey Branch, Newfoundland Department of Mines and Energy, Report* **93**, 1–15.

Chadwick B, Ramakrishnan M, Vasudev VN and Viswanatha MN (1989) Facies distributions and structure of a Dharwar volcanosedimentary basin: evidence for late Archaean transpression in southern India? *Journal of the Geological Society* **146**, 825–34.

Chadwick B, Vasudev VN and Hegde GV (2000) The Dharwar Craton, southern India, interpreted as the result of Late Archaean oblique convergence. *Precambrian Research* **99**, 91–111.

Chadwick B, Vasudev VN, Hegde GV and Nutman AP (2007) Structure and SHRIMP U/Pb zircon ages of granites adjacent to the Chitradurga schist belt: implications for Neoarchaean convergence in the Dharwar Craton, southern India. *Journal of Geological Society of India* **69**, 5–24.

Chardon D (1997) Les de´formations continentales arche´enes: examples naturales et mode´lisation thermomecanique Me´m. Doc. *Geosciences-Rennes* **76**, 300 pp.

Chardon D, Choukroune P and Jayananda M (1998) Sinking of the Dharwar basin (South India): implications for Archaean tectonics. *Precambrian Research* **91**, 15–39.

Chardon D and Jayananda M (2008) Three-dimensional field perspective on deformation, flow, and growth of the lower continental crust (Dharwar Craton, India). *Tectonics* **27**, TC1014.

Chardon D, Jayananda M, Chetty TR and Peucat JJ (2008) Precambrian continental strain and shear zone patterns: South Indian case. *Journal of Geophysical Research* **113**, B08402.

Chardon D, Peucat JJ, Jayananda M, Choukroune P and Fanning CM (2002) Archean granite-greenstone tectonics at Kolar (south India): interplay of diapirism and bulk inhomogeneous contraction during juvenile magmatic accretion. *Tectonics* **21**, 7–1.

Das A, Mallik J and Banerjee S (2021) Characterization of the magma flow direction in the Nandurbar-Dhule Deccan dyke swarm inferred from magnetic fabric analysis. *Physics of Earth and Planetary Interiors* **319**, 106782.

Datta S, Banerjee S, Samal AK and Srivastava RK (2023) Aspect ratio analysis of distinct Paleoproterozoicmafic dyke swarms and related fracture systems in the Eastern Dharwar Craton, India: implications for emplacement mechanism and depth of origin. *Physics of Earth and Planetary Interiors* **336**, 106998.

Dey S (2013) Evolution of Archaean crust in the Dharwar Craton: the Nd isotope record. *Precambrian Research* **227**, 227–46.

Droop G (1987) A general equation for estimating Fe3+ concentrations in ferromagnesian silicates and oxides from microprobe analyses, using stoichiometric criteria. *Mineralogical magazine* **51**, 431–5.

Drury SA, Harris NBW, Holt RW, Reeves-Smith GJ and Wightman RT (1984) Precambrian tectonics and crustal evolution in South India. *The Journal of Geology* **92**, 3–20.

Dunlop DJ and Özdemir O (1997) *Rock Magnetism: Fundamentals and Frontiers*. Cambridge, UK: Cambridge University Press, 573 p.

Elshaafi A and Gudmundsson A (2016) Volcano-tectonics of the Al haruj volcanic province, Central Libya. *Journal of Volcanology and Geothermal Research* **325**, 189–202.

Ernst RE (1994) Mapping the magma flow pattern in the Sudbury dyke swarm in Ontario using magnetic fabric analysis. *Current research, part E. Geological Survey of Canada* 183–92.

Ernst RE (2014) *Large Igneous Provinces*. Cambridge, UK: Cambridge University Press.

Ernst RE and Baragar WRA (1992) Evidence from magnetic fabric for the flow pattern of magma in the Mackenzie giant radiating dyke swarm. *Nature* **356**, 511–3.

Ernst RE, Grosfils EB and Mege D (2001) Giant dike swarms: earth, venus, and mars. *Annual Review of Earth and Planetary Science* **29**, 489–534.

Ernst RE and Srivastava RK (2008) India's place in the Proterozoic world: constraints from the Large Igneous Province (LIP) record. In *Indian Dykes: Geochemistry, Geophysics and Geochronology* (eds RK Srivastava, CH Sivaji and NVC Rao), pp. 41–56. New Delhi: Narosa Publ. House, Pvt. Ltd.

Ernst RE and Youbi N (2017) How Large Igneous Provinces affect global climate, sometimes cause mass extinctions, and represent natural markers in the geological record. *Palaeogeography Palaeoclimatology Palaeoecology* **478**, 30–52.

Fossen H (2016) *Structural Geology*. Cambridge, UK: Cambridge University Press.

French JE and Heaman LM (2010) U-Pb dating of Paleoproterozoic mafic dyke swarms of the south Indian Shield: implications for paleocontinental reconstructions and identifying ancient mantle plume events. *Precambrian Research* **183**, 416–41.

Gabbrosoft (2012) Ilmenite recalculation sheet. https://www.gabbrosoft.org/spreadsheets/.

Geoffroy L, Callot JP, Aubourg C and Moreira M (2002) Magnetic and plagioclase linear fabric discrepancy in dykes: a new way to define the flow vector using magnetic foliation. *Terra Nova* **14**, 183–90.

Gudmundsson A (2006) How local stresses control magma-chamber ruptures, dyke injections, and eruptions in composite volcanoes. *Earth Science Reviews* **79**, 1–31.

Halls HC, Kumar A, Srinivasan R and Hamilton MA (2007) Paleomagnetism and U–Pb geochronology of easterly trending dykes in the Dharwar Craton, India: feldspar clouding, radiating dyke swarms and the position of India at 2.37 Ga. *Precambrian Research* **155**, 47–68.

Hargraves RB, Johnson D and Chan CY (1991) Distribution anisotropy: the cause of AMS in igneous rocks? *Geophysical Research Letters* **18**, 2193–6.

Harish KS (2003) Late Archean juvenile magnetic accretion process in the eastern Dharwar Craton: Kuppam-Karimangalam area. *Memoires Geological Society of India* **50**, 375–408.

Hastie WW, Watkeys MK and Aubourg C (2014) Magma flow in dyke swarms of the Karoo LIP: implications for the mantle plume hypothesis. *Gondwana Research* **25**, 736–55.

Healy D, Rizzo R, Duffy M, Farrell NJ, Hole MJ and Muirhead D (2018) Field evidence for the lateral emplacement of igneous dykes: Implications for 3D mechanical models and the plumbing beneath fissure eruptions. *Volcanica* **1**, 85–105.

Hou G (2012) Mechanism for three types of mafic dyke swarms. *Geoscience Frontiers* **3**, 217–23.

Hou G, Wang C, Li J and Qian X (2006) Late Paleoproterozoic extension and a paleostress field reconstruction of the North China Craton. *Tectonophysics* **422**, 89–98.

Hrouda F (1982) Magnetic anisotropy of rocks and its application in geology and geophysics. *Geophysical surveys* **5**, 37–82.

Janák F (1965) Determination of anisotropy of magnetic susceptibility of rocks. *Studia Geophysica et Geodaetica* **9**, 290–301.

Jayananda M, Aadhiseshan KR, Kusiak MA, *et al.* (2020) Multi-stage crustal growth and Neoarchean geodynamics in the Eastern Dharwar Craton, southern India. *Gondwana Research* **78**, 228–60.

Jayananda M, Kano T, Peucat JJ and Channabasappa S (2008) 3.35 Ga komatiite volcanism in the western Dharwar Craton, southern India: constraints from Nd isotopes and whole-rock geochemistry. *Precambrian Research* **162**, 160–79.

Jayananda M and Mahabaleswar B (1991) Relationship between shear zones and igneous activity: the Closepet granite of Southern India. *Proceedings of the Indian Academy of Sciences-Earth and Planetary Sciences* **100**, 31–6.

Jayananda M, Moyen JF, Martin H, Peucat JJ, Auvray B and Mahabaleswar B (2000) Late Archean (2550–2520 Ma) juvenile magmatism in the Eastern Dharwar Craton, southern India: constraints from geochronology, Nd–Sr isotopes and whole rock geochemistry. *Precambrian Research* **99**, 225–54.

Jayananda M, Santosh M and Aadhiseshan KR (2018) Formation of Archean (3600–2500 Ma) continental crust in the Dharwar Craton, southern India. *Earth Science Review* **181**, 12–42.

Jayananda M, Tsutsumi Y, Miyazaki T, Gireesh RV, Kapfo KU, Hidaka H and Kano T (2013) Geochronological constraints on Meso-and Neoarchean regional metamorphism and magmatism in the Dharwar Craton, southern India. *Journal of Asian Earth Science* **78**, 18–38.

Jelinek V (1981) Characterization of the magnetic fabric of rocks. *Tectonophysics* **79**, T63–7.

Jourdan F, Féraud G, Bertrand H, Watkeys MK, Kampunzu AB and Le Gall B (2006) Basement control on dyke distribution in Large Igneous Provinces: case study of the Karoo triple junction. *Earth and Planetary Science Letters* **241**, 307–322.

Khan MA (1962) The anisotropy of magnetic susceptibility of some igneous and metamorphic rocks. *Journal of Geophysical Research* **67**, 873–2885.

Knight MD and Walker GP (1988) Magma flow directions in dikes of the Koolau Complex, Oahu, determined from magnetic fabric studies. *Journal of Geophysical Research: Solid Earth* **93**, 4301–19.

Kumar A, Nagaraju E, Besse J and Rao YB (2012) New age, geochemical and paleomagnetic data on a 2.21 Ga dyke swarm from south India: constraints on Paleoproterozoic reconstruction. *Precambrian Research* **220**, 123–38.

Kumar A, Parashuramulu V and Nagaraju E (2015) A 2082 Ma radiating dyke swarm in the Eastern Dharwar Craton, southern India and its implications to Cuddapah basin formation. *Precambrian Research* **266**, 490–505.

Kumar A, Rao YB, Sivaraman TV and Gopalan K (1996) Sm-Nd ages of Archaean metavolcanics of the Dharwar Craton, South India. *Precambrian Research* **80**, 205–16.

Launeau P and Cruden AR (1998) Magmatic fabric acquisition mechanisms in a syenite: results of a combined anisotropy of magnetic susceptibility and image analysis study. *Journal of Geophysical Research: Solid Earth* **103**, 5067–89.

Li SS, Santosh M and Palin RM (2018) Metamorphism during the Archean–Paleoproterozoic transition associated with microblock amalgamation in the Dharwar Craton, India. *Journal of Petrology* **59**, 2435–62.

Lowrie W and Fichtner A (2020) *Fundamentals of Geophysics*. Cambridge, UK: Cambridge University Press.

Maity S and Banerjee S (2022) Structural anatomy of the intraterrane shear zones in the archean Bundelkhand Craton, north-central India and its possible linkage to supercontinent assembly: Insights from field-and AMS-based kinematic analysis. *Lithosphere* **6**, 1–23.

Mandal B, Rao VV, Sarkar D, Bhaskar Rao YJ, Raju S, Karuppannan P and Sen MK (2018) Deep crustal seismic reflection images from the Dharwar Craton, Southern India—evidence for the Neoarchean subduction. *Geophysical Journal International* **212**, 777–94.

Manikyamba C and Kerrich R (2012) Eastern Dharwar Craton, India: continental lithosphere growth by accretion of diverse plume and arc terranes. *Geoscience Frontiers* **3**, 225–40.

Misra AA and Mukherjee S (2017) Dyke–brittle shear relationships in the western Deccan strike-slip zone around Mumbai (Maharashtra, India). *Geological Society of London: Special Publication* **445**, 269–95.

Mooney HM and Bleifuss R (1953) Magnetic susceptibility measurements in Minnesota; Part II, analysis of field results. *Geophysics* **18**, 383–93.

Moskowitz BM, Jackson MJ and Chandler VW (2015) Geophysical properties of the near surface earth: magnetic. In *Treatise on Geophysics* (ed G Schubert), vol. **2**, pp. 139–74. Amsterdam, Netherlands: Elsevier.

Nagaraju E and Parashuramulu V (2019) AMS studies on a 450 km long 2216 Ma dyke from Dharwar Craton, India: implications to magma flow. *Geoscience Frontiers* **10**, 931–1939.

Nagaraju E, Parashuramulu V, Kumar A and Sarma DS (2018) Paleomagnetism and geochronological studies on a 450 km long 2216 Ma dyke from the Dharwar Craton, southern India. *Physics of Earth and Planetary Interiors* **274**, 222–231.

Nagata T (1961) *Rock Magnetism*. Tokyo: Maruzen Company Ltd., **2**, 350 p.

Naqvi SM and Rogers JJW (1987) *Precambrian Geology of India*. New York: Oxford University Press.

Nilsson MKM, Klausen MB, Söderlund U and Ernst RE (2013) Precise U–Pb ages and geochemistry of Palaeoproterozoic mafic dykes from southern West Greenland: linking the North Atlantic and the Dharwar Cratons. *Lithos* **174**, 255–70.

Opdyke ND and Channell JE (1996) Magnetization processes and magnetic properties of sediments. *International geophysics* **64**, 26–48.

Parashuramulu V, Shankar R, Sarma DS, Nagaraju E and Babu NR (2021) Baddeleyite PbPb geochronology and paleomagnetic poles for~ 1.89–1.86 Ga mafic intrusions from the Dharwar Craton, India, and their paleogeographic implications. *Tectonophysics* **805**, 228789.

Parashuramulu V, Yadav P, Sarma DS and Babu NR (2022) Geochemistry of~ 2.08 Ga radiating mafic dyke swarm from the Dharwar Craton, India, and their implications on initiation of the Cuddapah Basin. *Journal of Earth System Science* **132**, 4.

Peucat JJ, Bouhallier H, Fanning CM and Jayananda M (1995) Age of the Holenarsipur greenstone belt, relationships with the surrounding gneisses (Karnataka, South India). *Journal of Geology* **103**, 701–10.

Peucat JJ, Mahabaleswar B and Jayananda M (1993) Age of younger tonalitic magmatism and granulitic metamorphism in the South Indian transition zone (Krishnagiri area); comparison with older Peninsular gneisses from the Gorur–Hassan area. *Journal of Metamorphic Geology* **11**, 879–88.

Piispa E, Smirnov AV, Pesonen LJ, Lingadevaru M, Anantha MKS and Devaraju TC (2011) An integrated study of Proterozoic dykes, Dharwar Craton, southern India. In *Dyke Swarms: Keys for Geodynamic Interpretation* (ed RK Srivastava), pp. 33–45. Berlin, Heidelberg: Springer.

Pivarunas AF and Meert JG (2020) IntraCratonic stability: a comparison of paleomagnetic data from the north and the south of Dharwar Craton, India. *Precambrian Research* **348**, 105858.

Pivarunas AF, Meert JG, Pandit MK and Sinha A (2018) Paleomagnetism and geochronology of mafic dykes from the Southern Granulite Terrane, India: expanding the Dharwar Craton southward. *Tectonophysics* **760**, 4–22.

Ramesh BN, Nagaraju E, Parashuramulu V and Venkateshwarlu M (2020) Preliminary anisotropy of magnetic susceptibility studies on 2367 Ma Bangalore-Karimnagar giant dyke swarm, southern India: implications for magma flow. *Physics of Earth and Planetary Interiors* **306**, 106540.

Rao VV, Murty ASN, Sarkar D, Rao YB, Khare P, Prasad ASSSRS, Sridher V, Raju S, Rao GSP, Kumar NP and Sen MK (2015) Crustal velocity structure of the Neoarchean convergence zone between the eastern and western blocks of Dharwar Craton, India from seismic wide-angle studies. *Precambrian Research* **266**, 282–95.

Raposo MIB and Ernesto M (1995) Anisotropy of magnetic susceptibility in the Ponta Grossa dyke swarm (Brazil) and its relationship with magma flow direction. *Physics of Earth and Planetary Interiors* **87**, 183–96.

Rasband WS (2012) *IMAGEJ, us National Institutes of Health*. Bethesda, MD, USA. http://imagej.nih.gov/ij/.

Rochette P, Jackson M and Aubourg C (1992) Rock magnetism and the interpretation of anisotropy of magnetic susceptibility. *Reviews of Geophysics* **30**, 209–26.

Samal AK, Rai AK and Srivastava RK (2021b) Multiple mantle melting events for two overlapping ca. 2.21–2.18 Ga mafic dyke swarms in the Dharwar Craton, India. International Geology Reviews 63, 2166–91.

Samal AK, Srivastava RK and Ernst RE (2021a) An appraisal of mineral systems associated with Precambrian Large Igneous Provinces of the Indian Shield. *Ore Geology Reviews* **131**, 104009.

Samal AK, Srivastava RK, Ernst RE and Söderlund U (2019a) Neoarchean-Mesoproterozoic mafic dyke swarms of the Indian Shield mapped using Google Earth™ images and ArcGIS™, and links with large igneous provinces. In *Dyke swarms of the World: A Modern Perspective* (eds RK Srivastava, RE Ernst and P Peng), pp. 335–90. Singapore: Springer.

Samal AK, Srivastava RK, Ernst RE and Söderlund U (2019b) Precambrian large igneous province record of the Indian Shield: an update based on extensive U-Pb dating of mafic dyke swarms. *LIP of the Month*.

Samal AK, Srivastava RK and Rahaman W (2021c) Sr-Nd isotope geochemistry and petrogenesis of ca. 2.26–2.25 Ga and ca. 2.08 Ga mafic dyke swarms from the Dharwar craton, India: insights into their mantle sources and geodynamic implications. *Lithos* **406**, 106503.

Sarma DS, Parashuramulu V, Santosh M, Nagaraju E and Babu NR (2020) Pb–Pb baddeleyite ages of mafic dyke swarms from the Dharwar Craton: implications for Paleoproterozoic LIPs and diamond potential of mantle keel. *Geoscience Frontiers* **11**, 2127–39.

Sen K and Mamtani MA (2006) Magnetic fabric, shape preferred orientation and regional strain in granitic rocks. *Journal of Structural Geology* **28**, 1870–82.

Söderlund U, Bleeker W, Demirer K, Srivastava RK, Hamilton M, Nilsson M, Pesonen LJ, Samal AK, Jayananda M, Ernst RE and Srinivas M (2019) Emplacement ages of Paleoproterozoic mafic dyke swarms in eastern Dharwar Craton, India: implications for paleoreconstructions and support for a~ 30° change in dyke trends from south to north. *Precambrian Research* **329**, 26–43.

Srivastava R (2011) *Dyke Swarms: Keys for Geodynamic Interpretation*. Heidelburg: Springer-Verlag.

Srivastava RK, Ernst RE, Buchan KL and de Kock M (2022a) An overview of the plumbing systems of large igneous provinces and their significance. *Geological Society of London, Special Publications* **518**, 1–16.

Srivastava RK, Ernst RE, Söderlund U, Samal AK, Pandey OP and Gautam GC (2022b) Existence of the Dharwar–Bastar–Singhbhum (DHABASI) megaCraton since 3.35 Ga: constraints from the Precambrian large igneous province record. *Geological Society of London, Special Publications* **518**, 173–96.

Srivastava RK, Jayananda M, Gautam GC, Gireesh V and Samal AK (2014b) Geochemistry of an ENE–WSW to NE–SW trending~ 2.37 Ga mafic dyke swarm of the eastern Dharwar Craton, India: Does it represent a single magmatic event? *Geochemistry* **74**, 251–65.

Srivastava RK, Jayananda M, Gautam GC and Samal AK (2014a) Geochemical studies and petrogenesis of~ 2.21–2.22 Ga Kunigal mafic dyke swarm (trending NS to NNW-SSE) from eastern Dharwar Craton, India: implications for Paleoproterozoic large igneous provinces and superCraton superia. *Mineral Petroleum* **108**, 695–711.

Srivastava RK, Samal AK, Ernst RE, Söderlund U and Shankar R (2020) Spatial and temporal distribution of Large Igneous Provinces in the Indian Shield–highlights of recent investigations. *Proceedings of the Indian National Science Academy* **86**, 313–30.

Srivastava RK, Samal AK and Gautam GC (2015) Geochemical characteristics and petrogenesis of four Palaeoproterozoic mafic dike swarms and associated large igneous provinces from the eastern Dharwar Craton, India. *International Geology Reviews* **57**, 1462–84.

Tarling DH and Hrouda F (1993) *The Magnetic Anisotropy of Rocks*. London: Chapman & Hall, 217 p.

Taylor PN, Chadwick B, Moorbath S, Ramakrishnan M and Viswanatha MN (1984) Petrography, chemistry and isotopic ages of Peninsular Gneiss, Dharwar acid volcanic rocks and the Chitradurga Granite with special reference to the late Archean evolution of the Karnataka Craton, southern India. *Precambrian Research* **23**, 349–75.

Torres-Hernández JR, Labarthe-Hernández G, Aguillón-Robles A, Gómez-Anguiano M and Mata-Segura JL (2006) The pyroclastic dikes of the Tertiary San Luis Potosí volcanic field: implications on the emplacement of Panalillo ignimbrite. *Geofísica internacional* **45**, 243–53.

Wiegand M, Trumbull RB, Kontny A and Greiling RO (2017) An AMS study of magma transport and emplacement mechanisms in mafic dykes from the Etendeka Province, Namibia. *Tectonophysics* **716**, 149–67.

Xu SS, Nieto-Samaniego AF and Alaniz-Álvarez SA (2013) Emplacement of pyroclastic dykes in Riedel shear fractures: an example from the Sierra de San Miguelito, central Mexico. *Journal of Volcanology and Geothermal Research* **250**, 1–8.

Yadav P and Sarma DS (2021) Geochemistry of 2.21 Ga giant radiating dyke swarm from the Western Dharwar Craton, India: Implications for petrogenesis and tectonic evolution. *Geological Journal* **56**, 3497–522.

Yadav P, Sarma DS and Parashuramulu V (2020) Pb-Pb baddeleyite ages of mafic dykes from the Western Dharwar Craton, Southern India: a window into 2.21–2.18 Ga global mafic magmatism. *Journal of Asian Earth Sciences* **191**, 104221.